

STRUCTURAL AND OPTICAL PROPERTIES EVALUATION OF
GOLD NANOPARTICLES VIA SYNTHESIS,
CHARACTERIZATION, MODELING AND SIMULATION

HANA ABDULLAH HAMED ALLUHAYBI

A thesis submitted in fulfilment of the
requirements for the award of the degree of
Doctor of Philosophy

Faculty of Science
Universiti Teknologi Malaysia

FEBRUARY 2021

DEDICATION

This thesis is especially dedicated to my beloved parents, my supportive husband (*Ahmed*). It is also dedicated to my sisters and brothers, my angels (*Aram, Lamar, Maryam, Marya*) and my soul (*Hamad*) and all my dearest friends. Thank you for your love and support.

ACKNOWLEDGEMENTS

In the name of Allah, the Most Gracious and Most Merciful. All praise to Allah S.W.T, the Almighty, who has provided us with the means of knowledge and to present this thesis.

I thank Allah - almighty for all the opportunities, health and blessings that enabled me to finish this dissertation. I am deeply humbled by every piece of knowledge that I learned. I hope that I would be able to acknowledge everyone who has sincerely made this work possible.

A very deep sincerely appreciation goes to my supervisor, Associate Prof. Dr. Sib Krishna Ghoshal, for his support, guidance, tolerance, humility in sharing his knowledge and precious time to discuss my thesis and for his endless helps throughout the years of study. I benefited a lot from our fruitful interactions and valuable discussions throughout this period.

I would like to express my gratitude to my co-supervisor, Dr. Wan Nurulhuda Wan Shamsuri, for her kindness, motivation and continuous encouragement throughout this research. She has provided a lot of assistance throughout this venture. I am also very thankful to my co-supervisor Dr. Bahia Alsobhi from Taibah University for her guidance, advices and motivation. Without their continued support and interest, this thesis would not have been the same as presented here.

A very warm and hearty acknowledgement goes to the late Dr. Osama Yaseen, may Allah be merciful to him. I have been very fortunate to have the opportunity to work with him over two years of my Ph.D. study before he passed away. I can honestly and confidently say that he has been a positive and helpful influence in my professional and personal life. I would like to express my most sincere gratitude to him, for his tireless dedication to his students and for his guidance and mentorship.

I am also indebted to Taibah University for funding my Ph.D study in its new programme (The Joint supervision programme between Taibah University and The UTM). Special thanks for the Department of Physics in UTM and staff for their assistance throughout the years.

Last but not least, deepest gratefulness and appreciation goes to my parents, husband and my family members for their support spiritually throughout my life, to whom this thesis is dedicated. Thanks are address to the Saudi Ministry of Education for the financial support given for me to pursue my Ph.D. Program here in the Universiti Teknologi Malaysia (UTM).

ABSTRACT

Gold nanoparticles (AuNPs) with customized morphologies, structures, optical and electronic properties for varied functional applications require an accurate synthesis and characterization technique. Furthermore, the basic understanding of these properties and validation of the experimental results depends on the precise modelling and first-principle density functional theory (DFT)-based simulations. In view of this, some AuNPs were prepared using the eco-friendly pulse laser ablation in liquid (PLAL) technique. As-grown AuNPs were characterized via diverse analytical tools including the ultraviolet-visible (UV-Vis) absorption, attenuated total reflectance (ATR), transmission electron microscopy (TEM), high-resolution transmission electron microscopy (HRTEM), Raman spectroscopy and photoluminescence (PL) spectroscopy. The influence of various laser parameters (laser energies, repetition rates, liquid environments, and laser wavelengths) on the structure, morphology, and optical traits of these AuNPs was determined. In addition, the first-principle DFT simulation was performed using WIEN2k software to complement the experimental results and explain the electronic structure properties of the produced AuNPs. For the first time, the spin-orbit coupling with the modified Becke-Johnson exchange potential (TB-mBJ) was included in the DFT framework for the band structure calculations of the AuNPs. A phenomenological model was also developed by integrating the effects of surface states and quantum confinement to describe the PL and absorption mechanism of AuNPs. The MATLAB code based on Mie-Gans theory was used to fit the experimental absorption data of AuNPs. By optimizing the laser parameters (especially the low laser energy ranging from 96.6 mJ up to 318 mJ, short pulse duration time of 3 min and low repetition rate of 1 Hz), the sizes of the spherical AuNPs were controlled in the deionized water (mean diameter of 7 to 30 nm) and ethanol (diameter of 3 to 6 nm) liquid medium. The strong UV-Vis absorption and surface plasmon resonance (SPR) peaks in the range of 521 to 529 nm accompanied by a blue-shift revealed by these AuNPs clearly indicated their effectiveness for sundry applications. The observed intense PL spectra of the studied AuNPs with optical band gap in the range of 2.95 to 3.9 eV were attributed to the effect of quantum-confinement. The obtained absorption characteristics, PL peak shifts, phonon energy dispersion in the Raman spectra, widening and broadening of the spectral peak due to the quantum size effects of AuNPs were validated using the model. The TEM images disclosed the formation of the colloidal AuNPs of average size ranged from 1 to 50 nm. Based on the WIEN2K simulation and experimental outcome of AuNPs, a structural and optical correlation was developed. The inclusion of spin-orbit coupling with the modified TB-mBJ potential in the DFT framework could more accurately predict the band structure (band gap energy) and shifts in the optical spectra of the proposed colloidal AuNPs compared to the existing reports. The achieved excellent fit of the experimental data with the model and simulation outcome in terms of bandgap and PL energy indicated the accuracy of the present method. It is established that the good quality colloidal AuNPs with tailored attributes can be produced by tuning the laser parameters of the PLAL technique. In short, the present study improved the prediction accuracy over the existing art-of-the techniques. This disclosure may contribute towards the development of spherical colloidal AuNPs useful for various applications.

ABSTRAK

Nanozarah emas (AuNPs) dengan morfologi, struktur, sifat-sifat optik dan elektronik yang disesuaikan untuk pelbagai aplikasi fungsian memerlukan teknik sintesis dan pencirian yang tepat. Selanjutnya, pemahaman asas mengenai sifat-sifat ini dan pengesahan hasil eksperimen bergantung pada pemodelan tepat dan simulasi berdasarkan teori kefungsiian ketumpatan (DFT) prinsip-pertama. Oleh itu, beberapa AuNPs disediakan dengan menggunakan teknik ablasi laser dalam cecair (PLAL) yang mesra alam. AuNPs telah dicirikan melalui pelbagai peralatan analisis termasuk penyerapan ultraungu-cahaya nampak (UV-Vis), pengurangan jumlah pantulan (ATR), mikroskopi elektron penghantaran (TEM), mikroskopi elektron penghantaran beresolusi tinggi (HRTEM), spektroskopi Raman dan spektroskopi fotoluminesen (PL). Pengaruh pelbagai parameter laser (tenaga laser, kadar pengulangan, persekitaran cecair, dan panjang gelombang laser) terhadap struktur, morfologi, dan sifat optik AuNP telah ditentukan. Di samping itu, simulasi DFT prinsip-pertama dilakukan menggunakan perisian WIEN2k untuk melengkapkan hasil eksperimen dan menjelaskan sifat-sifat struktur elektronik dari AuNP yang dihasilkan. Buat pertama kalinya, gandingan spin-orbit dengan keupayaan pertukaran Becke-Johnson yang diubah suai (TB-mBJ) telah diambil kira dalam kerangka DFT untuk pengiraan struktur jalur AuNPs. Satu model fenomenologi juga dibangunkan dengan menggabungkan kesan keadaan permukaan dan pengurangan kuantum untuk menggambarkan mekanisme PL dan penyerapan AuNP. Kod MATLAB berdasarkan teori Mie-Gans digunakan untuk menyesuaikan data penyerapan eksperimen AuNPs. Dengan mengoptimumkan parameter laser (terutamanya tenaga laser rendah berjulat dari 96.6 mJ hingga 318 mJ, jangka masa nadi pendek 3 min dan kadar pengulangan rendah 1 Hz), saiz AuNP sfera telah dikawal di dalam air ternyahion (min diameter cecair dari 7 hingga 30 nm) dan etanol (diameter dari 3 hingga 6 nm). Penyerapan UV-Vis yang kuat dan puncak permukaan resonans plasmon (SPR) di dalam julat 521 hingga 529 nm disertai dengan anjakan-biru yang ditunjukkan oleh AuNP ini jelas menunjukkan keberkesannya untuk pelbagai aplikasi. Spektrum PL kuat yang dicerap daripada AuNP yang dikaji dengan jurang jalur optik dalam julat 2.95 hingga 3.9 eV dikaitkan dengan kesan pengurangan kuantum. Ciri penyerapan yang diperolehi, anjakan puncak PL, penyebaran tenaga fonon dalam spektrum Raman, perluasan dan pelebaran puncak spektrum yang disebabkan oleh kesan saiz kuantum AuNPs dapat disahkan menggunakan model ini. Imej TEM mendedahkan pembentukan AuNP koloid dengan saiz purata berjulat daripada 1 hingga 50 nm. Berdasarkan simulasi WIEN2K dan hasil eksperimen AuNPs, korelasi struktur dan optik dapat dibangunkan. Rangkuman gandingan spin-orbit dengan keupayaan TB-mBJ yang diubah suai dalam kerangka DFT dapat meramal struktur jalur (jurang jalur tenaga) dan anjakan spektrum optik AuNP koloid yang dicadangkan dengan lebih tepat berbanding dengan laporan sedia ada. Penyesuaian data eksperimen yang dicapai dengan model dan hasil simulasi dari segi jurang jalur dan tenaga PL menunjukkan ketepatan kaedah ini. Telah dapat ditentukan bahawa AuNP koloid berkualiti tinggi dengan atribut yang disesuaikan boleh dihasilkan dengan menala parameter laser teknik PLAL. Secara ringkasnya, kajian ini meningkatkan ketepatan ramalan berbanding dengan teknik-teknik yang ada. Pendedahan ini dapat menyumbang ke arah perkembangan AuNP koloid sfera yang berguna untuk pelbagai aplikasi.

TABLE OF CONTENTS

	TITLE	PAGE
	DECLARATION	iii
	DEDICATION	iv
	ACKNOWLEDGEMENTS	v
	ABSTRACT	vi
	ABSTRAK	vii
	TABLE OF CONTENTS	viii
	LIST OF TABLES	xiv
	LIST OF FIGURES	xvii
	LIST OF ABBREVIATIONS	xxvi
	LIST OF SYMBOLS	xxvii
	LIST OF APPENDICES	xxviii
CHAPTER 1	INTRODUCTION	1
1.1	Research Background	1
1.1.1	Synthesis and Characterization of Gold Nanoparticles	2
1.1.2	Modelling of Optical and Structural Correlations of Gold Nanoparticles	4
1.1.3	Simulations of Electronic Structure Properties of Gold Nanoparticles	6
1.2	Problem Statement	8
1.3	Research Objectives	11
1.4	Scope of the Research	12
1.5	Significance of the Study	13
1.6	Novelty and Contributions	13
1.7	Thesis Organization	14
CHAPTER 2	LITERATURE REVIEW	17
2.1	Introduction	17

2.2	Structure and Properties of Bulk Gold	17
2.3	Structures and Properties of Gold Nanostructures	19
2.4	Localized Surface Plasmon Resonance (LSPR)	20
2.5	Gold Nanoparticles Synthesis Method	22
	2.5.1 Pulse Laser Ablation in Liquid (PLAL) Method	25
	2.5.2 Mechanisms of PLAL Growth Process	28
2.6	Characterization Techniques of Gold Nanoparticles	30
2.7	Dielectric Function of Au	35
	2.7.1 Models of Dielectric Function for Bulk Metals	36
	2.7.1.1 Basic Models	36
	2.7.1.2 Multi-Parameters Model	37
	2.7.1.3 Drude's Critical Points Model	40
2.8	Photoluminescence from Gold Nanostructures	43
	2.8.1 Quantum Confinement Effect (QCE)	46
	2.8.2 Localized Surface States (LSSs) Effect	48
2.9	Absorption of Gold Nanostructures	48
	2.9.1 Size Dependent Optical Properties	48
	2.9.2 Shape Dependent Optical Properties	51
	2.9.3 Optical Energy Band Gap and Absorption Coefficient of AuNPs	52
2.10	Theory and Model of AuNPs	53
	2.10.1 Density Functional Theory	53
	2.10.2 Relativistic Effect of AuNPs	56
2.11	WIEN2k Software for Electronic Structure Calculations	58
	2.11.1 Basis Function	59
	2.11.1.1 Augmented Plane Wave Method	59
	2.11.1.2 Linearized Augmented Plane Wave (LAPW) Method	60
	2.11.1.3 Full – Potential Linearized Augmented Plane Wave (FP-LAPW) Method	61

CHAPTER 3	RESEARCH METHODOLOGY	63
3.1	Research Framework	63
3.2	Gold Nanoparticles Preparation Using PLAL Method	65
3.3	Techniques for Samples Structure, Morphologies and Optical Characterizations	67
3.3.1	Morphological Analyses via High-Resolution Transmission Electron Microscopy	67
3.3.1.1	Image Processing with ImageJ software	68
3.3.2	Structural Characterization using Spectroscopy	69
3.3.2.1	Attenuated Total Reflection-Infrared Absorption Spectroscopy	69
3.3.2.2	Raman Spectroscopy	70
3.3.3	Characterizations for Optical Properties	71
3.3.3.1	Ultraviolet-Visible Absorption Spectroscopy	71
3.3.3.2	Photoluminescence Emission Spectroscopy	72
3.4	Phenomenological Modeling and Simulation	73
3.4.1	Formulation of the Model	73
3.4.2	Fitting Algorithm Using the MATLAB Code	76
3.5	DFT Calculation of the Electronic Band Structures using WIEN2k Software	79
3.5.1	Various Steps to Perform the DFT Simulation in WIEN2k	81
3.5.1.1	Generation of Structure	81
3.5.1.2	Initialization	82
3.5.1.3	SCF Calculations	82
3.5.2	Applications of the WIEN2K Code	83
3.5.2.1	Electronic Structure and Density of States (DOSs)	83
3.5.2.2	Theoretical Formulation for the Optical Properties	84

CHAPTER 4	EXPERIMENTAL RESULTS AND DISCUSSION	87
4.1	Introduction	87
4.2	Preparation of AuNPs in DIW using PLAL Method	87
4.3	Properties of AuNPs Grown in DIW	89
4.3.1	Laser Energy Dependent Morphology	89
4.3.1.1	Analysis using HRTEM Images	89
4.3.1.2	Pulse Repetition Rate Dependent Morphology of AuNPs	97
4.3.2	Structural Properties of AuNPs	104
4.3.2.1	ATR-IR Spectra of AuNPs	104
4.3.2.2	Raman Spectral Analysis of AuNPs	108
4.3.3	Optical Properties of AuNPs	113
4.3.3.1	Absorption Spectra of AuNPs	114
4.3.3.2	Photoluminescence Spectra of AuNPs	119
4.3.3.3	Laser Energy and Repetition Rate Dependent Optical Band Gap Energy of AuNPs	121
4.4	Preparation of AuNPs in Ethanol using PLAL Method	126
4.5	Properties of AuNPs Grown in Ethanol Media	128
4.5.1	Morphology Analysis using TEM	129
4.5.1.1	Laser Energy Dependent Morphology of AuNPs Grown at 1064 nm	129
4.5.1.2	Laser Energy Dependent Morphology of AuNPs Grown at 532 nm	135
4.5.2	Structural Properties of AuNPs	142
4.5.2.1	Laser Energy Dependent ATR-IR Spectra of AuNPs Grown at 1064 and 532 nm	142
4.5.2.2	Raman Spectral Analysis of AuNPs Grown at 1064 and 532 nm	147
4.5.3	Optical Properties of AuNPs Grown in Ethanol	151
4.5.3.1	Absorption Spectral Analyses	151

4.5.3.2	Evaluation of the Optical Band Gap Energies of AuNPs	156
CHAPTER 5	RESULTS AND DISCUSSION FOR MODELING AND SIMULATION	163
5.1	Introduction	163
5.2	Model Calculation for Photoluminescence Properties of Gold Nanoparticles	163
5.2.1	Size and Photon Energy Dependent Photoluminescence Traits of AuNPs	164
5.2.2	Fitting of Experimental PL Data with Model Calculated Spectra of AuNPs	168
5.3	Fitting of Model Simulation with Experimental Absorption Spectra of AuNPs	172
5.3.1	Mie-Gans Model Simulation Fitting with Experimental Absorbance of AuNPs	172
5.4	DFT Simulation Results on band Structures of AuNPs using WIEN2k Code	181
5.4.1	Structural and Optical Properties of Bulk Au	181
5.4.1.1	Initialization Steps in WIEN2k for Bulk Au	181
5.4.1.2	Electronic Band Structure for Bulk Au	182
5.4.1.3	Optical Properties of Bulk Au	187
5.4.2	DFT Simulation Results for Structural and Optical Properties of AuNPs	190
5.4.2.1	Initialization Steps in WIEN2k for the DFT Simulation of AuNPs	190
5.4.2.2	Size and Shape Dependent Electronic Band Structures of AuNPs	193
5.4.2.3	Dielectric Function of AuNPs	209
5.4.2.4	Absorbance Properties of AuNPs	211
CHAPTER 6	CONCLUSIONS AND RECOMMENDATIONS	217
6.1	Introduction	217
6.2	Conclusions	218
6.3	Recommendations	224

REFERENCES	227
LIST OF PUBLICATIONS	263

LIST OF TABLES

TABLE NO.	TITLE	PAGE
Table 2.1	Various nanomaterials synthesized via the PLAL method in different liquid media.	27
Table 2.2	Fitting Parameters for the dielectric function of bulk Au and bulk Ag (Rioux <i>et al.</i> , 2014).	42
Table 4.1	Details of the prepared AuNPs samples made in DIW and their codes as a function of laser energies and repetition rates.	88
Table 4.2	The laser ablation energy dependent average particle size, lattice fringe spacing and standard deviation of the prepared AuNPs.	96
Table 4.3	The laser pulse repetition rate dependent variation of the average particle size, lattice fringe spacing, standard deviation, and FWHM of the AuNPs.	103
Table 4.4	The AuNPs enhancement ATR-IR at different laser energies and repetition rates.	107
Table 4.5	Raman bands with their assignments for AuNPs prepared using PLAL method in DIW	111
Table 4.6	The average particle size obtained from the HRTEM and Raman spectral analyses.	112
Table 4.7	The laser parameters dependent UV-Vis absorption spectral traits of the PLAL grown AuNPs in DIW.	117
Table 4.8	Optical Band gap energy for AuNPs synthesized using varied laser parameters (energy and repetition rate).	124
Table 4.9	Details of the AuNPs samples and their codes prepared at room temperature in ethanol media under varying laser energies with two different laser wavelengths.	128
Table 4.10	The average particle size, lattice fringe spacing and the standard deviation of the AuNPs obtained using varying laser pulse energy in the ethanol media.	134
Table 4.11	The average particle size, the lattice fringe spacing, the standard deviation, and FWHM of the AuNPs obtained in ethanol media using varying laser pulse energy at the wavelength of 532 nm.	141

Table 4.12 The laser energy dependent ATR-IR spectral band position and assignments for the AuNPs prepared in ethanol media with 1064 nm and 532 nm wavelength.	145
Table 4.13 The Raman band position and assignments for the AuNPs prepared in ethanol with various laser pulse energies at the laser wavelength of 1064 and 532 nm.	149
Table 4.14 Comparison of the particle size obtained from the Raman spectral analysis with HRTEM estimates.	150
Table 4.15 The UV-Vis absorption spectral analysis of the AuNPs grown ethanol media.	155
Table 4.16 Laser energy dependent optical band gap energy of the AuNPs synthesized in ethanol medium at the wavelength of 1064 and 532 nm.	160
Table 5.1 Comparison of the model calculated PL parameters (for the main peak) with the experimentally measured one of the AuNPs grown in DIW at different laser energies.	169
Table 5.2 Comparison of the model calculated PL parameters (for the main peak) with the experimentally measured one of the AuNPs grown in DIW at different laser pulse repetition rates.	170
Table 5.3 Comparison of the experimental optical absorption properties of the AuNPs grown in DIW at various LAEs with Mie-Gans model simulation fitting (using MATLAB programming).	176
Table 5.4 Comparison of the experimental optical absorption properties of the AuNPs grown in DIW at various laser RRs with Mie-Gans model simulation fitting (using MATLAB programming).	180
Table 5.5 Comparison of the present energy eigenvalues (in eV) at high symmetry points in the first Brillouin zone of bulk Au with other state-of-the-art techniques.	186
Table 5.6 Lattice parameters for the spherical and non-spherical AuNPs chosen for the DFT simulation.	192
Table 5.7 The DFT simulated structural and optical parameters of the spherical AuNPs.	195
Table 5.8 The DFT simulated structural and optical parameters for the non-spherical AuNPs	196
Table 5.9 Inter-band and intra-band transitions along L symmetric point and X symmetric point for the spherical AuNPs calculated using non-relativistic PBE and relativistic TB-mBJ.	203
Table 5.10 Inter-band and intra-band transitions along L symmetric point and X symmetric point for the non- spherical AuNPs	

calculated using non-relativistic PBE and relativistic TB-mBJ.	203
Table 5.11 Energy eigenvalues for different sizes of the spherical AuNPs along the high symmetry points in the first Brillouin zone under the effect of non-relativistic PBE function.	205
Table 5.12 Energy eigenvalues for different sizes of the spherical AuNPs along the high symmetry points in the first Brillouin zone under the effect of relativistic PBE plus TBmBJ function.	206
Table 5.13 Energy eigenvalues for different sizes of non-spherical AuNPs along high symmetry points in the first Brillouin zone under the effect of non-relativistic PBE function.	207
Table 5.14 Energy eigenvalues for different sizes of non-spherical AuNPs along the high symmetry points in the first Brillouin zone under the effect of relativistic PBE plus TBmBJ function.	208
Table 5.15 A comparison of the theoretically evaluated absorbance of the spherical AuNPs of different sizes with the experimentally measured absorbance of the AuNPs prepared using PLAL method at various LAEs.	214
Table 5.16 A comparison of the theoretically evaluated absorbance of the non-spherical AuNPs of different sizes with the experimentally measured absorbance of the AuNPs prepared using PLAL method at various laser energies.	216

LIST OF FIGURES

FIGURE NO.	TITLE	PAGE
Figure 1.1	Concept map of the thesis.	8
Figure 1.2	Chapter content flowchart of the thesis.	14
Figure 2.1	General physical properties of bulk Au.	18
Figure 2.2	Bulk Au electronic structure, The arrows show the inter-band gap between the highest occupied 5d band (red line) and the lowest unoccupied 6sp bands (blue lines), The Fermi level is set to 0 (dashed-black line) (Rangel <i>et al.</i> , 2012).	19
Figure 2.3	The geometric and the electronic structures of single atom, clusters, and nanoparticles (Liu and Corma, 2018).	20
Figure 2.4	LSPR of AuNPs resulting from the collective oscillation of delocalized electrons in response to an external electric field (Cobley <i>et al.</i> , 2011).	21
Figure 2.5	Schematic of the preparative methods of NPs.	23
Figure 2.6	Experimental set-up of pulsed laser ablation in liquid media (Zhang <i>et al.</i> , 2017b).	24
Figure 2.7	The main stages of the PLAL process. The white arrows indicate that upon increasing the distance from the laser spot, the temperature (T), pressure (P) and concentration of the ablated material (C_M) decrease, while the concentration of solution species (C_S) increases (Amendola and Meneghetti, 2013)	28
Figure 2.8	Sketch of the ablation process with nanosecond laser pulses. The upper illustration shows the formation of two shock waves, the plasma plume, the cavitation bubble, and nucleation, as well as the growth of nanomaterials and the locations of their formation during PLAL at different stages (Amendola and Meneghetti, 2013)	29
Figure 2.9	Low and high resolution TEM images and corresponding FFT images for AuNPs (Liu <i>et al.</i> , 2019).	31
Figure 2.10	(a) Raman spectra of crystal violet and (b) and (c) Raman spectra with Au and Ag nanoparticles, prepared using laser ablation with 1064 nm and 355 nm laser, as substrates (Vinod and Gopchandran, 2014).	32
Figure 2.11	TEM images of: (a) 13 nm; and (b) 50 nm spherical (AuNPs); and (c) rod shaped (AuNRs); (d) their UV/Visible	

spectra; and (e) images of corresponding colloidal suspensions (Altunbek <i>et al.</i> , 2016).	34
Figure 2.12 Imaginary part of the dielectric function. Experimental data adapted from Johnson and Christy (1972); Palik (1998) and compared with calculated values from Drude model, critical model and the Derkachova model	39
Figure 2.13 (a) Structure of Au (blue) and Ag (red) near the critical points at the: (a) X and (b) L symmetry points. The green arrows at X represent the threshold (ω_{01}) and gap (ω_{g1}) transitions from the d-bands to the s-band above the Fermi level. The green arrows at L represent the threshold (ω_{02}) and gap (ω_{g2}) transitions from the s-band below the Fermi level to energy levels above it. The orange arrow at L represents the threshold (ω_{03}) transition from the d bands to the s band above the Fermi level (Rioux <i>et al.</i> , 2014).	42
Figure 2.14 Comparison of the critical model (Eq. 2.10) with experimental data for imaginary parts of the $\epsilon\omega$ and the corresponding parameters are shown in Table 2.2.	43
Figure 2.15 Processes involved in the photoluminescence of Au nanostructures (Andersen <i>et al.</i> , 2015).	44
Figure 2.16 Schematic model of inter-band excitation and emission (Huang and Murray, 2001).	45
Figure 2.17 Quantum size effect on the band gap and the density of states as the number of atoms in a system increases (from right to left) where δ is the so-called Kubo gap (Roduner, 2006).	47
Figure 2.18 The unit cell volume partitioned into the muffin-tin (MT) spheres (S) and the interstitial region (I).	60
Figure 3.1 The flowchart of the research methodology.	64
Figure 3.2 Schematic presentation of the PLAL setup for the AuNPs synthesis from Au target ablation immersed in the liquid (facility available at Laser Centre of UTM).	66
Figure 3.3 Schematic diagram of the HRTEM structure (http://www.hkphy.org/atomic_world/tem/tem02_e.html)	68
Figure 3.4 Schematic layout of the ATR-FTIR spectrometer (Ausili <i>et al.</i> , 2015).	69
Figure 3.5 Schematic layout of the Raman spectroscopic instrument (https://courses.lumenlearning.com/labmethods/chapter/part-of-a-raman-spectrometer)	71
Figure 3.6 Schematic diagram showing the layout of the UV-Vis-NIR spectroscopy.	72

Figure 3.7 Schematic diagram showing the layout of the PL spectroscopy (https://www.edinst.com/blog/what-is-a-spectrophotometer)	73
Figure 3.8 The flowchart for the fitting procedure of the experimentally recorded absorption spectrum.	78
Figure 3.9 Pictorial presentation of the solution of Schrodinger equation within the DFT framework.	80
Figure 3.10 The generation of the unit cell structure with lattice parameters in the code.	81
Figure 4.1 Photographs of the eight samples of AuNPs suspension prepared by PLAL method in the DIW with different: (a) laser pulse energies, and (b) repetition rates.	88
Figure 4.2 The PLAL synthesized AuNPs in DIW obtained with the lowest laser energy of 96.6 mJ: (a) low resolution TEM image, (b) AuNPs size distribution, (c) HRTEM image of the selected AuNP, (d) corresponding FFT pattern of the marked rectangular part and (e) lattice fringe profile.	90
Figure 4.3 The PLAL grown AuNPs in DIW obtained with the pulse laser energy of 226 mJ: (a) low resolution of TEM image, (b) size distribution, (c) HRTEM image, (d) FFT pattern of the marked rectangular part of the AuNP and (e) corresponding lattice fringe profile.	92
Figure 4.4 The PLAL grown AuNPs in DIW obtained with the pulse laser energy of 286 mJ and fixed repetition rate of 1 Hz: (a) low resolution of TEM image, (b) size distribution, (c) HRTEM image, (d) FFT pattern of the marked rectangular part of the AuNP and (e) corresponding lattice fringe profile.	93
Figure 4.5 The AuNPs morphology grown in DIW using pulse laser energy of 318 mJ: (a) a top view image of the AuNPs, (b) AuNPs size distribution, (c) HRTEM image, (d) FFT pattern of the marked rectangular part of AuNP and (e) Lattice fringe profile.	95
Figure 4.6 The lattice spacing, average particle size and standard deviation of the AuNPs prepared in DIW (y-axis) against ablation energy (x-axis).	97
Figure 4.7 The AuNPs growth in DIW using repetition rate of 2 Hz: (a) low resolution of TEM image, (b) AuNPs size distribution, (c) HRTEM image, (d) FFT pattern of the marked rectangular part of AuNP and (e) Lattice fringe profile.	98
Figure 4.8 The AuNPs morphology grown in DIW using repetition rate of 4 Hz: (a) a top view image of the AuNPs, (b) AuNPs size distribution, (c) HRTEM image, (d) FFT pattern of the	

marked rectangular part of AuNP and (e) Lattice fringe profile.	100
Figure 4.9 PLAL synthesized AuNPs in DIW obtained with 6 Hz repetition rate: (a) top view of TEM image, (b) AuNPs size distribution, (c) HRTEM image, (d) FFT pattern of the marked rectangular part of AuNP and (e) Lattice fringe profile.	101
Figure 4.10 The evolution of the AuNPs morphology in DIW as a function of repetition rate of 8 Hz: (a) top view of TEM image, (b) AuNPs size distribution, (c) HRTEM image, (d) FFT pattern of the marked rectangular part of AuNP and (e) Lattice fringe profile.	102
Figure 4.11 Laser pulse repetition rate dependent morphological properties (lattice spacing, average particle size and standard deviation) of the AuNPs prepared in DIW.	103
Figure 4.12 The room temperature ATR-IR spectra of the PLAL grown AuNPs at different laser energy of (a) 96.6 mJ, (b) 226 mJ, (c) 286 mJ and (d) 318 mJ.	105
Figure 4.13 The ATR-IR spectra of the AuNPs as a function of repetition rate of (a) 2 Hz, (b) 4 Hz, (c) 6 Hz and (d) 8 Hz.	106
Figure 4.14 The Raman spectra of the AuNPs produced in DIW at different laser energies.	109
Figure 4.15 Raman spectra of the PLAL synthesized AuNPs obtained with different repetition rates.	110
Figure 4.16 Comparison of the AuNPs size obtained by the HRTEM with the one obtained from Raman spectra for varying (a) laser energy and (b) repetition rate.	113
Figure 4.17 The room temperature UV–Vis absorption spectra of the AuNPs obtained at varying laser pulse of (a) 96.6 mJ, (b) 226 mJ, (c) 286 mJ and (d) 318 mJ.	115
Figure 4.18 The room temperature UV–Vis absorption spectra of the AuNPs obtained at varying repetition rates of (a) 2 Hz, (b) 4 Hz, (c) 6 Hz and (d) 8 Hz.	116
Figure 4.19 Laser parameters dependent absorption spectral properties of the AuNPs prepared in DIW at different (a) laser energy and (b) repetition rate.	118
Figure 4.20 Photoluminescence spectra of the AuNPs at different pulse energies of (a) 96.6 mJ, (b) 226 mJ, (c) 286 mJ and (d) 318 mJ. Insets show the band gap energy values measured from the intense PL spectral peak.	120

- Figure 4.21** Photoluminescence spectra of the AuNPs at different repetition rates of (a) 2 Hz, (b) 4 Hz, (c) 6 Hz and (d) 8 Hz. Insets show the band gap energy values measured from the intense PL spectral peak. 121
- Figure 4.22** Evaluation (using Tauc plot) of the optical band gap energy of the AuNPs synthesized at different laser energies of (a) 96.6 mJ, (b) 226 mJ, (c) 286 mJ and (d) 318 mJ. Insets show the E_g values measured from the intense PL spectral peak. 122
- Figure 4.23** Evaluation (using Tauc plot) of the optical band gap energy of the AuNPs synthesized at different repetition rates of (a) 2 Hz, (b) 4 Hz, (c) 6 Hz and (d) 8 Hz. Insets show the E_g values measured from the intense PL spectral peak. 123
- Figure 4.24** The values of E_g of the AuNPs versus different laser parameters (a) laser energy and (b) repetition rate. 126
- Figure 4.25** The photographs of the AuNPs samples prepared by PLAL method in the ethanol media with different laser energy at the fixed wavelength: (a) 1064 nm and (b) 532 nm. 127
- Figure 4.26** The AuNPs morphology grown in ethanol using pulse ablation energy of 96.6 mJ: (a) a top view TEM image of the AuNPs, (b) AuNPs size distribution, (c) HRTEM image, (d) FFT pattern of the marked rectangular part of AuNP and (e) Lattice fringe profile. 130
- Figure 4.27** The AuNPs growth in C_2H_5-OH media using pulse laser energy of 226 mJ: (a) low resolution of TEM image, (b) AuNPs size distribution, (c) HRTEM image, (d) FFT pattern of the marked rectangular part of AuNP and (e) Lattice fringe profile. 131
- Figure 4.28** The evolution of the AuNPs morphology in ethanol as a function of laser energy (286 mJ) at fixed repetition rate (1 Hz): (a) top view of TEM image, (b) AuNPs size distribution, (c) HRTEM image, (d) FFT pattern of the marked rectangular part of AuNP and (e) Lattice fringe profile. 132
- Figure 4.29** The AuNPs morphology grown in ethanol liquid media using pulse energy of 318 mJ: (a) a top view image of the AuNPs, (b) AuNPs size distribution, (c) HRTEM image, (d) FFT pattern of the marked rectangular part of AuNP and (e) Lattice fringe profile. 133
- Figure 4.30** The lattice spacing, average particle size and standard deviation of the AuNPs synthesized in ethanol as a function of the laser energy. 135
- Figure 4.31** PLAL synthesized AuNPs in ethanol media obtained with laser fundamental wavelength of 532 nm and laser energy of 96.6 mJ: (a) top view of TEM image, (b) AuNPs size

distribution, (c) HRTEM image, (d) FFT pattern of the marked rectangular part of AuNP, (e) Lattice fringe profile.	136
Figure 4.32 The evolution of the AuNPs morphology in ethanol as a function of pulse energy (226 mJ) at laser wavelength (532 nm): (a) top view of TEM image, (b) AuNPs size distribution, (c) HR-TEM image, (d) FFT pattern of the marked rectangular part of AuNP and (e) Lattice fringe profile.	138
Figure 4.33 The AuNPs morphology grown in C ₂ H ₅ -OH media using pulse laser energy of 286 mJ and laser wavelength of 532 nm: (a) a top view image of the AuNPs, (b) AuNPs size distribution, (c) HRTEM image, (d) FFT pattern of the marked rectangular part of AuNP, (e) Lattice fringe profile.	139
Figure 4.34 The AuNPs growth in ethanol using pulse laser energy of 318 mJ and a fundamental laser wavelength 532 nm: (a) low resolution of TEM image, (b) AuNPs size distribution, (c) HRTEM image, (d) FFT pattern of the marked rectangular part of AuNP and (e) Lattice fringe profile.	140
Figure 4.35 Laser pulse energies dependent properties for AuNPs prepared in ethanol media at fundamental laser wavelength 532 nm: (a) average particle size, (b) standard deviation and (c) lattice spacing.	142
Figure 4.36 The ATR-IR spectra of the PLAL grown AuNPs at different laser energy of: (a) 96.6 mJ, (b) 226 mJ, (c) 286 mJ and (d) 318 mJ.	143
Figure 4.37 The ATR-IR spectra of the AuNPs prepared with varying pulse ablation energy at fixed laser wavelength of 532 nm.	144
Figure 4.38 The room temperature Raman spectra of the AuNPs prepared in ethanol media at different laser energies with 1064 nm wavelength.	147
Figure 4.39 The room temperature Raman spectra of the AuNPs prepared in ethanol media at different laser energies with 532 nm wavelength.	148
Figure 4.40 The laser energy dependent AuNPs particle size obtained from the HRTEM and Raman spectral analyses at the wavelength of (a) 1064 nm and (b) 532 nm.	151
Figure 4.41 The UV-Vis absorption spectra of the AuNPs in ethanol media prepared with 1064 nm at varying laser pulse energy of (a) 96.6 mJ, (b) 226 mJ, (c) 286 mJ and (d) 318mJ.	153
Figure 4.42 The UV-Vis absorption spectra of the AuNPs in ethanol media prepared with 532 nm at varying laser pulse energy of (a) 96.6 mJ, (b) 226 mJ, (c) 286 mJ and (d) 318mJ.	154

- Figure 4.43** Laser energy dependent intense SPR absorption peak position, intensity, and FWHM for the AuNPs prepared in ethanol media at the wavelength of (a) 1064 nm and (b) 532 nm. 156
- Figure 4.44** The evaluation of the optical band gap energy for AuNPs grown in ethanol media at different laser energy: (a) 96.6 mJ, (b) 226 mJ, (c) 286 mJ and (d) 318 mJ. 157
- Figure 4.45** The dependence of $(\alpha h\nu)^2$ on photon energy ($h\nu$) for the prepared AuNPs in ethanol at a fundamental laser wavelength of 532 nm and different pulse ablation. 158
- Figure 4.46** AuNPs optical band gap energies obtained using different laser energies in Ethanol media: (a) laser wavelength 1064 nm and (b) Laser wavelength 532 nm. 161
- Figure 5.1** The PL spectra computed for AuNPs with different values of L_0 and different standard deviation (σ) 165
- Figure 5.2** The computed PL spectra of the AuNPs with normal size distribution, different L_0 and fixed $\sigma = 10\%$ of L_0 166
- Figure 5.3** The computed normalized PL spectra of the AuNPs for the fixed normal size distribution, $L_0 = 7.1$ nm and $\sigma = 0.71$ nm with three different values of γ (a measure of the oscillator strength). 167
- Figure 5.4** The computed PL spectra of the AuNPs obtained with different size distribution and $L_0 = 7.1$ nm 168
- Figure 5.5** Experimental PL spectra (solid blue line) fitted to the model simulated spectra (red dotted line) for the AuNPs samples: (a) GLW-1, (b) GLW-2, (c) GLW-3 and (d) GLW-4. 169
- Figure 5.6** Experimental PL spectra (solid blue line) fitted to the model simulated spectra (red dotted line) for the AuNPs samples: (a) GRW-1, (b) GRW-2, (c) GRW-3 and (d) GRW-4. 171
- Figure 5.7** Left panel shows the experimental absorption spectra (black solid line) fitted with the Mie-Gans model simulated spectra using MATLAB program (red dotted line) of the AuNPs grown in DIW at the LAE of (a) 96.6 mJ, (b) 226 mJ, (c) 286 mJ, and (d) 318 mJ. Right panel displays the HRTEM images of the AuNPs and the corresponding size distribution (inset) fitted with a normal distributions curve (red line). 174
- Figure 5.8** Left panel shows the experimental absorption spectra (black solid line) fitted with the Mie-Gans model simulated spectra using MATLAB program (red dotted line) of the AuNPs grown in DIW at the laser energy of (a) 2 Hz, (b) 4 Hz, (c) 6 Hz and (d) 8 Hz. Right Panel displays the HRTEM images of

the AuNPs and the corresponding size distribution (inset) fitted with a normal distributions curve (red line).	178
Figure 5.9 (a) The electronic band structures at various symmetry points, and (b) total DOSs of bulk Au calculated using PBE (blue solid curves) and PBE+SOC (red dashed curves). Inset-1a and Inset-1b displays the lowest inter-band and intra-band transitions along the respective L-point and X-point obtained via PBE and relativistic PBE.	183
Figure 5.10 (a) Electronic band structures at various symmetry points, and (b) the total DOSs of bulk Au calculated using TBmBJ (blue solid curves) and TBmBJ+SOC (red dashed curves). Inset-2a and Inset-2b depicts the lowest inter-band and intra-band transitions along the respective L-point and X-point obtained via TBmBJ and relativistic TBmBJ.	185
Figure 5.11 Energy dependent imaginary part of the dielectric function for bulk Au obtained using (a) PBE and PBE+SOC function and (b) TBmBJ and TBmBJ+SOC function when compared with the experimental findings.	189
Figure 5.12 The variation of the lattice parameter (ap) as the function of diameter (D) of the AuNPs.	193
Figure 5.13 (a) Electronic band structures and (b) TDOSs of the spherical AuNPs of diameter 1 nm.	198
Figure 5.14 (a) Electronic band structures and (b) TDOSs of the spherical AuNPs of diameter 2 nm.	199
Figure 5.15 (a) Electronic band structures and (b) TDOSs of the spherical AuNPs of diameter 7 nm.	199
Figure 5.16 (a) Electronic band structures and (b) TDOSs of the spherical AuNPs of diameter 45 nm.	200
Figure 5.17 (a) Electronic band structures and (b) TDOSs of the non-spherical AuNPs of diameter 1 nm.	201
Figure 5.18 (a) Electronic band structures and (b) TDOSs of the non-spherical AuNPs of diameter 2 nm.	201
Figure 5.19 (a) Electronic band structures and (b) TDOSs of the non-spherical AuNPs of diameter 7 nm.	202
Figure 5.20 (a) Electronic band structures and (b) TDOSs of the non-spherical AuNPs of diameter 45 nm.	202
Figure 5.21 Spherical AuNPs size dependent (1 nm, 2 nm, 7 nm, and 45 nm) imaginary part of the complex dielectric function calculated using : (a) PBE function and (b) TBmBJ+SOC approximation.	210

- Figure 5.22** Non-spherical AuNPs size dependent (1 nm, 2 nm, 7 nm, and 45 nm) imaginary part of the complex dielectric function calculated using: (a) PBE function and (b) TBmBJ+SOC approximation. 211
- Figure 5.23** Spherical AuNPs size dependent absorption spectra calculated using the (a) PBE function and (b) TBmBJ + SOC approximation. Inset: LAE dependent experimental absorption spectra of AuNPs. 213
- Figure 5.24** Non-spherical AuNPs size dependent absorption spectra calculated using the (a) PBE function and (b) TBmBJ + SOC approximation. Inset: LAE dependent experimental absorption spectra. 215

LIST OF ABBREVIATIONS

Au	-	Gold
Ag	-	Silver
AuNPs	-	Gold Nanoparticles
NPs	-	Nanoparticles
DFT	-	Density Functional Theory
PLAL	-	Pulsed Laser Ablation in Liquid
DIW		Deionized water
LAE		Laser ablation energies
TEM	-	Transmission Electron Microscopy
HRTEM	-	High-Resolution Transmission Electron Microscopy
FTIR	-	Fourier Transform Infrared
ATR-IR	-	Attenuated total reflection infrared
UV/Vis	-	Ultraviolet/Visible Spectroscopy
PL	-	Photoluminescence
QC	-	Quantum Confinement
LSSs	-	Localized surface states
KS	-	Kohn-Sham
LDA	-	The Local-Density Approximation
GGA	-	Generalized Gradient Approximation
PBE	-	Perdew, Burke, and Ernzerhof
TB	-	Tran and Blaha
TB-mBJ	-	The Becke-Johnson Potential Modified by Tran and Blaha
FP-LAPW	-	The Full-Potential Linearized Augmented Plane Wave Method
LAPW	-	Linearized Augmented Plane Wave
LP-PLA	-	Liquid Phase Pulsed Laser Ablation
SOC	-	Spin-orbit Coupling
SCF	-	Self-consistent field
SPR	-	Surface plasmon resonance
CPs	-	Critical points

LIST OF SYMBOLS

χ_c	-	The exchange–correlation
ϵ	-	The dielectric function
n	-	Refractive index
γ	-	Relaxation frequency
l_e	-	Electron mean free path l_e
ϵ_∞	-	Dielectric constant
λ	-	The wavelength
ω	-	The frequency
ω_p	-	Bulk plasma frequency
C_{ext}	-	The extinction cross-section
C_{sca}	-	The scattering
C_{abs}	-	The absorption
v_F	-	Fermi velocity
E_F	-	Fermi energy
R	-	The aspect ratio
E_g	-	Optical band gap energy
$\rho(r)$	-	The electron charge density
β and α	-	Quantum confinement model constants
$I(\Delta E_{d,s})$	-	PL intensity
σ	-	Standard deviation

LIST OF APPENDICES

APPENDIX	TITLE	PAGE
Appendix A	Dielectric function of gold nanoparticles	243
Appendix B	MATLAB Code for Mie-Gans fitting simulations	245

CHAPTER 1

INTRODUCTION

This chapter identifies the remaining issues involving the gold nanoparticles (AuNPs) and clarifies the need of the present study in this field. The motivation for the experimental and theoretical investigations addressing the past developments, present activities and future trends on the AuNPs are also highlighted as background. The goals and objectives of the undertaken thesis are explained. The research workflows, methodology, scopes, and significance are discussed.

1.1 Research Background

Currently, the AuNPs have attracted significant research interests (fundamental and applied) because of their unique size- and shape-dependent (morphological) properties beneficial for diverse purposes (De Souza *et al.*, 2019; Kayang *et al.*, 2019; Laban *et al.*, 2020). These unique properties have led to many significant potential technological applications and have opened new (challenging) opportunities for the nanoscience and nanotechnology. In particular, the correlation among the structural, physical, and optical properties of the small size AuNPs (at nanoscale) is not clearly understood (Luo *et al.*, 2019; Shabaninezhad and Ramakrishna, 2019). The morphologies of the AuNPs prepared using varieties of synthesis techniques show wide variations depending on the method used. On top, it has been realized that the optical, electrical, and physical properties of these nanoscale gold particles are decided by their structure and morphology (Amendola *et al.*, 2014). Thus, an in-depth theoretical understanding is necessary for the diverse application of these NPs, where modeling and simulation play a vital role. So far, a comprehensive phenomenological model for the evaluation of such properties of the grown AuNPs has been lacking. Despite many experimental studies and some model

calculations (Derkachova *et al.*, 2016; Zhang *et al.*, 2017b; De Souza *et al.*, 2019), the detail theoretical understanding of the correlation among structural, physical, and optical properties of the AuNPs is far from being achieved.

As aforementioned, the renewed interest in the AuNPs arises from their unique structural, physical, and optical properties that enable using them in the diverse settings (Taghizadeh *et al.*, 2019; Vedhanayagam *et al.*, 2019). In the last 50 years, much research has been focused into the production of the AuNPs with controlled morphology (sizes and shapes) where different system parameters of the growth processes are adjusted to achieve the optimum properties (Frens, 1973; Hong and Li, 2013; Laban *et al.*, 2020). The AuNPs with desirable size in the range of 10 μm to 1 nm were prepared from the reliable and high-yield techniques (Zhang *et al.*, 2017a). However, the enhancement of the production accuracy for the much-desired growth of these nanoparticles remains demanding. In addition, the theoretical perceptive or knowledge on the mechanism behind the distinctive optical properties of these NPs is still incomplete (Pattabi and Pattabi, 2014; Cai *et al.*, 2018). A complete model for these NPs that include the surface state and quantum confinement effects is relatively a new area needs to be explored, wherein the simulation of such model can bring a better understanding of the mechanisms related to various properties. On the other hand, most of the theoretical formulations and modelling using the first-principle density functional theory (DFT)-based calculations are still ongoing for the bulk gold (Kurelchuk *et al.*, 2017; Matrane *et al.*, 2018). Therefore, considering the immense fundamental and applied significance of AuNPs it can be asserted that there is a pressing need for more intensive research on their experimental and theoretical understanding. To achieve this goal the present research work is conducted.

1.1.1 Synthesis and Characterization of Gold Nanoparticles

Over the years, many techniques have been introduced to prepare the AuNPs of tiny sizes such as the physical irradiation (Dehghani *et al.*, 2017), laser ablation (Rafique *et al.*, 2017), chemical reduction (De Souza *et al.*, 2019), sol-gel

(Kobayashi *et al.*, 2001), and biological (such as microorganisms, plants) (Ahmed *et al.*, 2016). However, in spite of some advantages of each such technique most of them suffers from some limitations, including the difficulty in controlling the nanoparticles morphology (shape and size), sustainability, stability, yield, reproducibility, separations, narrow distribution and surface functionalizations with other chemical species. Furthermore, the production of the contaminant-free AuNPs with acceptable morphology and desired characteristics is an essential requirement for further investigations and developments in the field.

In recent times, the optical methods for synthesizing various types of organic and inorganic NPs has attracted wide interest because of their accuracy in adjusting system parameters, eco-friendliness, simplicity, cost-effectiveness, high yield, scalability, tunable morphology, non-requirement of extra chemicals, and the ability to produce contaminant free nanoparticles with desired properties (Zeng *et al.*, 2012; Lee *et al.*, 2020). In this regard, the pulsed laser ablation in liquid (PLAL) due to its simplicity and low cost has emerged as one of the most versatile green methods for producing ultrafine NPs with outstanding purity and unique surface chemistry in the form of highly stable colloidal suspension (Giorgetti *et al.*, 2012). The PLAL is also an adaptable and environmental friendly approach for obtaining varieties of the impurity-free nanoparticles with the desired morphologies. Since its inception, the PLAL method has been used to improve the structures and morphologies of different types of nanostructures (Yan and Chrisey, 2012). The results obtained from the PLAL technique were shown to be highly promising for the diverse potential applications, wherein various operational parameters related to the laser and other conditions can be adjusted to improve the experimental outcome (Zhang *et al.*, 2017a). These controlled conditions include the laser parameters such as the type of laser source, pulse wavelength, duration, energy, fluence, and repetition rate (Amendola and Meneghetti, 2013), nature of the liquid species (Riabinina *et al.*, 2012), physical conditions (Dell'Aglio *et al.*, 2016), and growth chamber design (Maciulevičius *et al.*, 2013). Compared to other chemical and physical methods, the PLAL technique for the production of various nanoparticles has advantages related to purity, simplicity and morphology improvement.

The morphological characterizations of the grown ultra-fine AuNPs are usually performed using transmission electron microscopy (TEM) and high-resolution transmission electron microscopy (HRTEM). Thus, the HRTEM has become an essential image analysis tool for obtaining the precise size and distribution of AuNPs. The structural properties (vibrational modes) of the AuNPs related to the different functional groups can accurately be determined using the Fourier transform infrared (FTIR) and Raman spectral analyses. In contrast to bulk Au, the AuNPs have higher visible absorption and scattering cross-sections (in the spectral range near 520 nm) depending on their surface plasmon absorption spectra (Kreibig and Vollmer, 2013; Link and El-Sayed, 1999). These unique features of the AuNPs make them suitable to study their optical traits by the ultraviolet/visible (UV/Vis) spectroscopy (Wang *et al.*, 2014). In addition, the photoluminescence (PL) emission attributes of the AuNPs that is extremely significant from the applied viewpoint can be analyzed using the PL spectroscopy (Mooradian, 1969). Actually, the PL measurement provides the vital information about the direct and indirect optical band gaps, radiative recombination of the d electrons with holes near the Fermi level, quantum size effects and the allowed optical transitions. Although intensive research has been directed towards the preparation, structural and optical properties of the AuNPs, very few studies have explored their correlations in terms of the basic mechanisms behind these properties. Thus, together with the experimental studies on the AuNPs there is a need to develop model and perform simulation to complement the theoretical predictions on various properties and their correlations.

1.1.2 Modelling of Optical and Structural Correlations of Gold Nanoparticles

Photoluminescence emission traits of the AuNPs have intensively been investigated in the past decade because of their potential applications in different fields of engineering, technology and biomedicine (Carattino *et al.*, 2018; Nedyalkov *et al.*, 2019). Various structural parameters such as the nanoparticle sizes (ranging from 0.3 to 20 nm), surface ligands/attached functional groups, and valence states

have been tuned to synthesise high quality luminescent AuNPs (Pattabi and Pattabi, 2014; Cai *et al.*, 2018). Some theoretical studies have been conducted to understand the effects of these factors on the luminescence emission mechanisms of the AuNPs and to further improve as well as predict the PL properties (Zheng *et al.*, 2012). However, the incorporation of the quantum confinement (QC) and surface state effects of the AuNPs of varying sizes in an analytical model that can predict the experimentally observed PL spectra and optical band gap energy of the AuNPs is still deficient.

An analytical PL model (also called phenomenological model) based on the effects of the QC and localised surface states (LSSs) has been proposed for the semiconductor (especially nanosilicon) with finite band gap energies (Islam and Kumar, 2003; Isiyaku and Ghoshal, 2016). In this perception, it is believed that the quantum confinement effects mediated by the discrete energy levels in the metal NPs can lead to a great improvement in the PL model and further simulation outcome especially the electronic structure properties. The prediction of the exact mechanism of the visible PL emission from the metal NPs with diverse morphologies based on the reliable theoretical model simulation is essential for fundamental knowledge and various applications. An accurate calculation of the PL spectra of the AuNPs with various shapes and sizes (different morphologies) can be made to verify the experimental observation. Nevertheless, the UV/Vis absorption spectra have already been modelled for different particle sizes, shapes, and concentrations of the AuNPs that are known to have strong dependence on the surface plasmon resonance (SPR) effects (Amendola and Meneghetti, 2009; Affandi *et al.*, 2015).

The UV/Vis spectroscopy enables the characterisation of the content in an AuNPs suspension by fitting the spectra according to the Mie model for the spherical particles and the Gans model for the spheroidal particles (Link and El-Sayed, 1999; Amendola and Meneghetti, 2009; Affandi *et al.*, 2015). The calculation of these optical properties is possible with a numerical solution depending on the dielectric function $\varepsilon(\omega)$ of the materials. The dielectric functions incorporated in the analytical Mie-Gans model for the pure elements such as the Au and silver (Ag) [$\varepsilon(Au)$ and $\varepsilon(Ag)$] have been obtained for the bulk metal (Amendola and Meneghetti, 2009;

Affandi *et al.*, 2015). By merging the nano-dialectic function with the inter-band transitions in the analytical model for the absorption properties of the AuNPs, it is possible to gain some new insights for controlling and predicting the optical properties of the AuNPs in a customised way. An accurate understanding of different optical and physical properties and thereby establishing their correlation requires a thorough investigation of the electronic band structure properties of the AuNPs. It can be attained using the first principle DFT-based simulations and subsequent validation with the experimental results.

1.1.3 Simulations of Electronic Structure Properties of Gold Nanoparticles

It is worth mentioning that the theoretical determination of the electronic band structures of the bulk Au has been an open issue for more than five decades (Rangel *et al.*, 2012). The remarkable physical properties of the Au especially the oxidation resistance make it one of the few materials capable of withstanding long-term exposure to the atomic oxygen atmosphere. This characteristic makes Au a standard material to protect spacecraft and satellite parts, a property that was famously exploited to make the golden records on the Voyager spacecraft (Jones *et al.*, 2013). Despite the similarity in the crystal structure and atomic radius between Au and Ag, the atomic-scale mechanism of Au has attracted great interest for gaining a fundamental understanding of the unique properties of bulk Au.

For more than 30 years, first-principle DFT has been successfully used for the parameter-free description of the electronic band structure calculations and properties related to the total energy. These characteristics via total energy minimization include the equilibrium volume, elastic constants, and phonon frequencies of any solid, can be predicted with reasonable precision (Glantschnig and Ambrosch-Draxl, 2010). Numerous approximation techniques have been proposed for enhancing the calculation accuracies of the Kohn-Sham (KS) Hamiltonian equation. Amongst these methods the most commonly used are of the local-density approximation (LDA), generalized gradient approximation (GGA), and Perdew, Burke, and Ernzerhof

(PBE) approximations (Koller *et al.*, 2012). The GGA overcomes many shortcomings of the LDA, especially for the systems with strong variations in the electron density and provides reasonable results that are comparable with the experiments (Matrane *et al.*, 2018). One of the shortcomings of both the LDA and GGA is the poor estimation of the band gap value (Baida and Ghezali, 2018). Thus, to enhance the accuracy of the calculated properties, different effects and approximations must be considered.

Within the framework of KS-DFT, many difficulties that exist with the LDA/GGA can be overcome. Recently, Tran and Blaha (TB) have proposed a meta-GGA type local potential that is built on the early work by Becke and Johnson which has been termed as the TB-mBJ potential (Koller *et al.*, 2012). By applying to a comprehensive set of semiconductors, the Tran and Blaha showed that the TBmBJ potential can give remarkably accurate band gaps with a computational effort comparable to that of the LDA/GGA calculation (Tran and Blaha, 2009). Based on this rationale, the TB-mBJ approach has been further extended to different types of materials (Jiang, 2013; Benatia *et al.*, 2018; Özdemir and Merdan, 2020). However, the results obtained using the TB-mBJ potential for the metallic material has shown poor accuracy (Koller *et al.*, 2011). Although many studies (Theileis and Bross, 2000; Dal Corso and Conte, 2005; Glantschnig and Ambrosch-Draxl, 2010) have attributed the observed remarkably varying physical properties of the bulk Au to the huge influence of the relativistic effects, hardly any accurate calculations of the structural and optical properties have been performed for further validation. It has been inferred that the implementation of the full relativistic effect with the most recent TB-mBJ potential for the bulk Au might give an accurate prediction of the structural and optical properties. Moreover, the correlation between the experimental results and first principle DFT-based calculation for the AuNPs can be validated through the model simulation. In this view, the present work investigates the structural and optical properties of the AuNPs via synthesis, characterization, theoretical formulation, modeling and simulation. Figure 1.1 illustrates the overall design for the thesis.

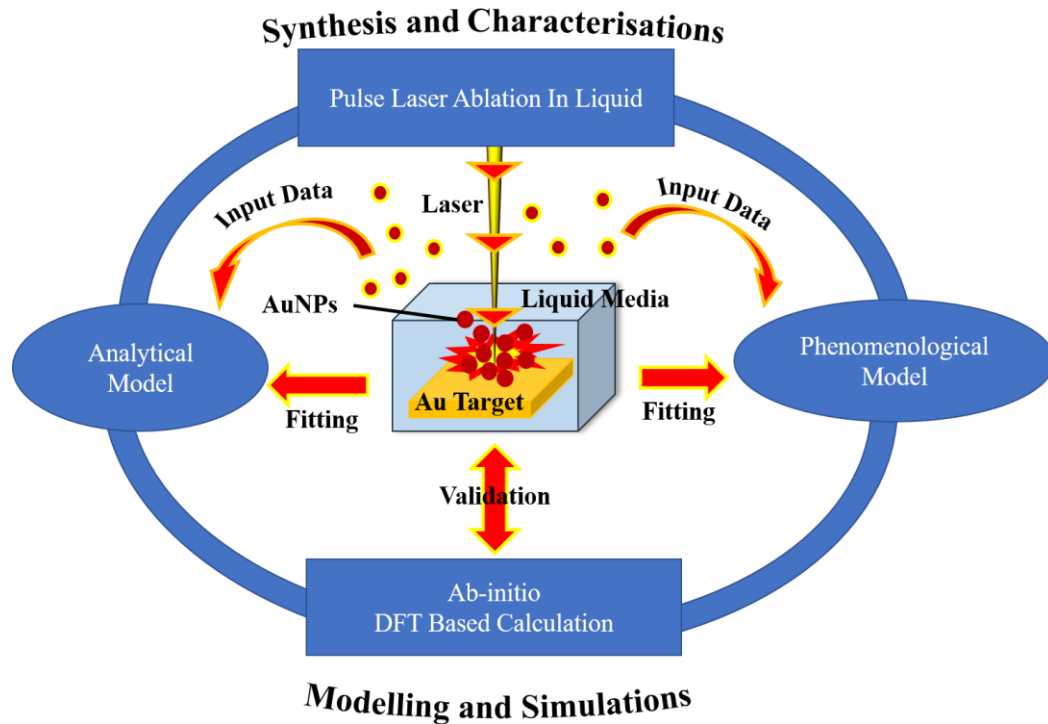


Figure 1.1 Concept map of the thesis.

1.2 Problem Statement

As mentioned previously, although several methods have been developed over the years to synthesize the AuNPs of desirable sizes, morphologies, and distributions for varied applications however there is a need for the accurate and eco-friendly technique to produce pure AuNPs (Bhattarai *et al.*, 2018; Nayef and Khudhair, 2018; Liu *et al.*, 2019). Considering the advantages and disadvantages of these preparation methods for the production of the accurate colloidal AuNPs with purity, the optical techniques show much more promise (Zhang *et al.*, 2017b; Choudhury *et al.*, 2019). Very few studies have used PLAL to synthesize AuNPs (Dell’Aglia *et al.*, 2016; Palazzo *et al.*, 2017; Rafique *et al.*, 2017). Recent reports revealed that (Zhang *et al.*, 2017a; Vinod *et al.*, 2017; Yu *et al.*, 2017) using the PLAL technique it is possible to control and optimize the structure, morphology, and various other properties (for example the physical, optical, and chemical) of the AuNPs by varying different laser-related parameters (such as the laser energy, time duration, repetition rate, and laser wavelength) together with the growth media, physical conditions, and chamber design. Most of the earlier works (Vinod and Gopchandran, 2014; Affandi *et al.*, 2015; Rafique *et al.*, 2017) are focused to

produce the AuNPs in the size range of 9.5 to 49 nm. However, to the best of the present authors' knowledge no studies have been dedicated to prepare tiny AuNPs using the low energy pulse laser ablation and short pulse durations with the frequency in the intermediate range. It is expected that such variations in the laser parameters are not only suitable for achieving the desirable morphology and structure of the AuNPs but also can lead to the better control and tunability towards the production process to yield contaminant-free, good quality, and accurate NPs with narrow size distributions.

A comprehensive literature review indicated that for any kind of NP (organic or inorganic) application, the systematic and in-depth characterizations of the diverse properties (physical, structural, morphological, optical, and electronic structures) are prerequisite. The optical, structural, and morphological characteristics of the PLAL-grown NPs (produced at higher energy fluencies) have recently been reported (Dell'Aglio *et al.*, 2016; Palazzo *et al.*, 2017; Yu *et al.*, 2017). However, the production possibilities of the AuNPs in the regime of the intermediate energy (moderate laser fluence) and low time duration have not been inspected. In addition, none of the existing reports showed any correlation between the structural, morphological, optical and electronic structure properties of the PLAL-grown NPs. Only systematic characterizations using diverse measurements and comprehensive analyses of the experimental data using various mechanisms can provide a better understanding of the PLAL-grown AuNPs. Therefore, more experimental efforts together with the theoretical formalisms are needed to enhance the AuNPs database.

The experimental data concerning the optical properties of the diverse metallic and semiconducting nanostructures have been modeled using different techniques by incorporating the effects of the quantum confinement and surface states separately. The main aim of these developed models was to explain the fluorescence spectra, absorption data, and band gaps (Lin *et al.*, 2016; Cai *et al.*, 2018). However, none of these models have been applied to the Au nanostructures for explaining their optical and electronic structure properties. Experimental reports suggest that most of the optical properties of AuNPs are decided by the quantum confinement and surface state (Kumar, 2013). The surface states in combination with

the quantum confinement effect have been identified as the versatile and successful model to explain the PL properties of the semiconductor nanostructures (Islam and Kumar, 2003; Isiyaku and Ghoshal, 2016). Therefore, this model with some modifications can be applied to explain the optical properties of the AuNPs. So far, none of the reports has been indicated to apply such a model on the spherical NPs grown via the PLAL method. Subsequent simulations of the model with various parameters, such as average particle size, peak energy, NP distributions, peak position and width might lead to better fits of the experimental data for the AuNPs that are not yet performed. However, the legitimacy of the developed model needs to be validated via the comparison with another state-of-the-art technique, particularly the first principle-based DFT calculations.

The first-principle-based DFT is the most popular one among the diverse electronic band structure calculation schemes (Glantschnig and Ambrosch-Draxl, 2010; Suárez *et al.*, 2016). Various algorithms and different types of functionals such as the non-empirical, minimal empirical and over empirical have been developed. The development of these formalisms led to the easy availability of different functionals and approximations. Non-empirical functionals such as the LDA and GGAs are reliable for predicting the electronic structure properties of the new systems. However, these functionals often produce systematic errors and that need to be corrected. Recently, the DFT has been applied to produce properties of the bulk Au and Au nanostructures (Dal Corso and Conte, 2005; Glantschnig and Ambrosch-Draxl, 2010). Glantschnig and Ambrosch-Draxl (2010) have produced the scalar-relativistic terms in the DFT calculations and observed a great disagreement between the theoretical and experimental results. It is believed that to enhance the electronic structure, further investigations concerning the exchange-correlation (xc) effects need to be conducted (Koller *et al.*, 2011; Nainaa and Ez-Zahraouy, 2018). It is important to mention that not much accurate simulations have been performed on the band structure of AuNPs using the first-principle DFT-based calculations. Thus, the present thesis propose to use the celebrated WIEN2K codes with the recent xc potential called the Becke-Johnson potential modified by Tran and Blaha (TBmBJ) and the scalar-relativistic terms to bridge the gap between theory and experiment. Although the WIEN2K simulations and DFT have been used to simulate a variety of the metallic nanostructures for their electronic structure properties, systematic DFT

calculations concerning the colloidal spherical gold NPs are still lacking. By validating the simulation data with the experimental and modeling results, it is possible to develop an interrelationship among the structural, optical, morphological, and electronic structure properties. In short, despite the different synthetic technique of producing AuNPs, different models for explaining their overall properties, different characterization techniques for better analysis of the NPs, and various simulations including the DFT to validate the experimental- and model- calculated data are still lacking. On top, no conclusive remarks on the optical properties of the AuNPs have been made so far.

The above-mentioned facts clearly indicate that the careful synthesis, characterizations, phenomenological modeling, and first-principle DFT-based simulations concerning the colloidal AuNPs are critically important. Based on these research gaps, the following objectives are set to resolve some of the existing issues related to the PLAL-grown colloidal AuNPs.

1.3 Research Objectives

The following research objectives were identified:

1. To synthesize spherical the AuNPs using the PLAL method with various laser parameters and liquid media.
2. To characterize the synthesized AuNPs for their structural, morphological and optical properties.
3. To determine the structural and optical properties correlation of these AuNPs by developing a phenomenological model and subsequent MATLAB simulation.
4. To validate the model by comparing with experimental findings and first-principle DFT-based calculations on the structural and optical properties of AuNPs.

To accomplish these objectives, several methods and techniques have been employed as described in the scope of the study.

1.4 Scope of the Research

As mentioned above, the main objectives of the thesis are to prepare the AuNPs using the PLAL technique and then to characterize the as-grown AuNPs using diverse analytical techniques. Next, the experimental data need validation using a comprehensive phenomenological model and comparison of the results with the experimental data and accurate DFT-based calculations. To achieve these objectives, several steps were considered:

1. Preparation of the AuNPs using the PLAL techniques with various laser parameters, especially using the intermediate energies.
2. Structural characterization using HRTEM, FTIR, ATR, and Raman spectroscopy.
3. Determination of the optical properties using UV/Vis absorption and fluorescence spectroscopy.
4. Development of a phenomenological model by incorporating the quantum size effects and surface states.
5. Simulation of the model using MATLAB coding to determine the structural and optical properties of AuNPs of varying shape and size.
6. Validation of the model by comparing with the achieved experimental results and other findings.
7. MATLAB programming of the model for calculating the AuNPs size and shape-dependent structural and optical properties.
8. Determination of the structural and optical properties using the first-principle DFT based simulation using WIEN2K software.

9. Fitting of the experimental data on the morphology-dependent structural and optical properties of AuNPs with the phenomenological model via the MATLAB programming.

1.5 Significance of the Study

This study is of interest to both fundamental and applied researchers in terms of synthesis, characterization, modeling and simulation of high-quality AuNPs, which are needed for many applications. Besides, the understanding of the structural and optical properties is significant for development of new applications. The knowledge on the modeling and simulation can play vital roles in fulfilling the experimental gap and linking experimental data to theories. Recent progress in the plasmonic NPs reveals that they have the prospect for diverse application in science, technology, and engineering. In this view, the present work is going to accomplish the set objectives and resolve the existing issues related to AuNPs. The phenomenological modeling and subsequent simulation are expected to bridge the gap between the theory and experiments. The first-principle DFT-based simulations would make accurate quantitative predictions about the structural and optical properties of the AuNPs. This work is expected to develop a better insight into the shape- and size-dependent optical and structural properties of spherical AuNPs.

1.6 Novelty and Contributions

This thesis investigates various properties of the colloidal AuNPs starting from the synthesis, modeling, theory and simulation. The main novel contributions of this research project consist of several findings:

- i. Use of different laser parameters such as the intermediate laser energy, low repetition rate, and very short duration time to produce the AuNPs with desired morphology.

- ii. The incorporation of the dielectric function for the spherical AuNPs in the modeling for the implementation in the scattering theory.
- iii. Integrations of the quantum confinement and the surface state in the comprehensive phenomenological model for the AuNPs to predict the PL spectra of the synthesized spherical AuNPs
- iv. The enhancement of the AuNPs in the DFT calculations via the application of the relativistic terms with the recent potential of the Becke-Johnson potential modified by Tran and Blaha (TBmBJ) to calculate an accurate structural and optical properties for AuNPs.
- v. The evaluation of a structural and optical correlation in the AuNPs for the first time.

1.7 Thesis Organization

This thesis is divided into several chapters. An overview of the thesis chapters is given in Figure 1.2



Figure 1.2 Chapter content flowchart of the thesis.

In chapter 1, general background information concerning the fundamental and experimental techniques for synthesizing AuNPs is given. The objectives, significance, and the problems are also described.

Chapter 2 provides a detailed literature review on the theory of DFT-based calculations in addition to the theory of optical AuNP properties. The review includes a description of the Mie-Guns modelling for the absorbance property of AuNPs.

In Chapter 3, the research methods, experimental setup, procedures, different laser parameters, and experimental techniques for collecting data are explained. This chapter also includes a description of the modelling system used in this study for determining the phenomenological model. The software-based setup for the DFT simulations is included as part of each chapter.

Chapter 4 discusses the experimental results of the synthesized AuNPs. The optimum growth conditions are identified. Different laser dependent parameters were studied and discussed.

In Chapter 5, the theoretical results are discussed. The comprehensive phenomenological model for absorbance and luminescence properties was explored. Structural and optical DFT calculations were also made for the AuNPs. The correlation between the experimental results and the theoretical calculations were validated.

Finally, conclusions drawn from the discussion and overall outcomes of this research are described in Chapter 6. The possibilities of extending the present model in the future are also described.

REFERENCES

- Abràmoff, M.D., Magalhães, P.J. and Ram, S.J. (2004) 'Image processing with ImageJ', *Biophotonics International*, 11(7), pp.36-42.
- Adams, S. and Zhang, J.Z. (2016) 'Unique optical properties and applications of hollow gold nanospheres (HGNs)', *Coordination Chemistry Reviews*, 320, pp.18-37.
- Affandi, M.S., Bidin, N., Abdullah, M., Aziz, M.S.A., Al-Azawi, M. and Nugroho, W. (2015) 'In situ measurement of gold nanoparticle production', *Journal of Nanophotonics*, 9(1), p.093089.
- Agulló-Rueda, F., Mendez, E.E., Bojarczuk, B. and Guha, S. (2000) 'Raman spectroscopy of wurtzite InN films grown on Si', *Solid State Communications*, 115(1), pp.19-21.
- Ahmed, S. and Ikram, S. (2016) 'Biosynthesis of gold nanoparticles: a green approach', *Journal of Photochemistry and Photobiology B: Biology*, 161, pp.141-153.
- Alaqad, K. and Saleh, T.A. (2016) 'Gold and silver nanoparticles: synthesis methods, characterization routes and applications towards drugs', *Journal of Environmental and Analytical Toxicology*, 6(4), pp.525-2161.
- Al-Azawi, M.A. and Bidin, N. (2015) 'Gold nanoparticles synthesized by laser ablation in deionized water', *Chinese Journal of Physics*, 53(4), pp.201-209.
- Altunbek, M., Kuku, G. and Culha, M. (2016) 'Gold nanoparticles in single-cell analysis for surface enhanced Raman scattering', *Molecules*, 21(12), p.1617.
- Ambrosch-Draxl, C. and Sofo, J.O. (2006) 'Linear optical properties of solids within the full-potential linearized augmented planewave method', *Computer Physics Communications*, 175(1), pp.1-14.
- Amendola, V. and Meneghetti, M. (2009) 'Size evaluation of gold nanoparticles by UV–vis spectroscopy', *The Journal of Physical Chemistry C*, 113(11), pp.4277-4285.
- Amendola, V. and Meneghetti, M. (2013) 'What controls the composition and the structure of nanomaterials generated by laser ablation in liquid solution?', *Physical Chemistry Chemical Physics*, 15(9), pp.3027-3046.

- Amendola, V., Meneghetti, M., Stener, M., Guo, Y., Chen, S., Crespo, P., García, M.A., Hernando, A., Pengo, P. and Pasquato, L. (2014) 'Physico-chemical characteristics of gold nanoparticles', *In Comprehensive Analytical Chemistry* (Vol. 66, pp. 81-152). Elsevier.
- Amendola, V., Pilot, R., Frasconi, M., Maragò, O.M. and Iatì, M.A. (2017) 'Surface plasmon resonance in gold nanoparticles: a review', *Journal of Physics: Condensed Matter*, 29(20), p.203002.
- Amendola, V., Polizzi, S. and Meneghetti, M. (2006) 'Laser ablation synthesis of gold nanoparticles in organic solvents', *The Journal of Physical Chemistry B*, 110(14), pp.7232-7237.
- Andersen, O.K. (1975) 'Linear methods in band theory', *Physical Review B*, 12(8), p.3060.
- Andersen, S.K., Pors, A. and Bozhevolnyi, S.I. (2015) 'Gold photoluminescence wavelength and polarization engineering', *Acs Photonics*, 2(3), pp.432-438.
- Ausili, A., Sánchez, M. and Gómez-Fernández, J.C. (2015) 'Attenuated total reflectance infrared spectroscopy: A powerful method for the simultaneous study of structure and spatial orientation of lipids and membrane proteins', *Biomedical Spectroscopy and Imaging*, 4(2), pp.159-170.
- Baida, A. and Ghezali, M. (2018) 'Structural, electronic and optical properties of InP under pressure: An ab-initio study', *Computational Condensed Matter*, 17, p.e00333.
- Benatia, M., Driss-Khodja, F.Z., Saadaoui, F., Driss-Khodja, M. and Boudali, A. (2018) 'Structural, elastic, thermodynamic, and electronic properties of BaHfO₃: A first-principles study using GGA-PBEsol+ TB-mBJ approach', *Computational Condensed Matter*, 16, p.e00296.
- Bhattacharai, B., Zaker, Y. and Bigioni, T.P. (2018) 'Green synthesis of gold and silver nanoparticles: Challenges and opportunities', *Current Opinion in Green and Sustainable Chemistry*, 12, pp.91-100.
- Bhuyan, B., Paul, A., Paul, B., Dhar, S.S. and Dutta, P. (2017) 'Paederia foetida Linn. promoted biogenic gold and silver nanoparticles: synthesis, characterization, photocatalytic and in vitro efficacy against clinically isolated pathogens', *Journal of Photochemistry and Photobiology B: Biology*, 173, pp.210-215.

- Blaha, P., Schwarz, K., Sorantin, P. and Trickey, S.B. (1990) 'Full-potential, linearized augmented plane wave programs for crystalline systems', *Computer Physics Communications*, 59(2), pp.399-415.
- Bohren, C.F. and Huffman, D.R. (2004) 'Absorption and scattering of light by small particles', *John Wiley & Sons*.
- Cai, Y.Y., Liu, J.G., Tauzin, L.J., Huang, D., Sung, E., Zhang, H., Joplin, A., Chang, W.S., Nordlander, P. and Link, S. (2018) 'Photoluminescence of gold nanorods: Purcell effect enhanced emission from hot carriers', *Acs Nano*, 12(2), pp.976-985.
- Car, R. (2002) 'Introduction to Density-Functional Theory and ab-Initio Molecular Dynamics', *Quantitative Structure-Activity Relationships*, 21(2), pp.97-104.
- Carattino, A., Caldarola, M. and Orrit, M. (2018) 'Gold nanoparticles as absolute nanothermometers', *Nano letters*, 18(2), pp.874-880.
- Cederquist, K.B., Liu, B., Grima, M.R., Dalack, P.J. and Mahorn, J.T. (2017) 'Laser-fabricated gold nanoparticles for lateral flow immunoassays', *Colloids and Surfaces B: Biointerfaces*, 149, pp.351-357.
- Chartier, G. (2005) 'Introduction to optics', *Springer Science & Business Media*.
- Choudhury, K., Singh, R.K., Kumar, P., Ranjan, M., Srivastava, A. and Kumar, A. (2019) 'Effect of confined geometry on the size distribution of nanoparticles produced by laser ablation in liquid medium', *Nano-Structures & Nano-Objects*, 17, pp.129-137.
- Christensen, N.E. and Seraphin, B.O. (1971) 'Relativistic band calculation and the optical properties of gold', *Physical Review B*, 4(10), p.3321.
- Cobley, C.M., Chen, J., Cho, E.C., Wang, L.V. and Xia, Y. (2011) 'Gold nanostructures: a class of multifunctional materials for biomedical applications', *Chemical Society Reviews*, 40(1), pp.44-56.
- Courths, R., Zimmer, H.G., Goldmann, A. and Saalfeld, H. (1986) 'Electronic structure of gold: An angle-resolved photoemission study along the Λ line', *Physical Review B*, 34(6), p.3577.
- Dal Corso, A. and Conte, A.M. (2005) 'Spin-orbit coupling with ultrasoft pseudopotentials: Application to Au and Pt', *Physical Review B*, 71(11), p.115106.

- De Souza, C.D., Nogueira, B.R. and Rostelato, M.E.C. (2019) 'Review of the methodologies used in the synthesis gold nanoparticles by chemical reduction', *Journal of Alloys and Compounds*, 798, pp.714-740.
- Deepak, F.L., Mayoral, A. and Arenal, R. eds. (2015) 'Advanced transmission electron microscopy: Applications to nanomaterials', *Springer*.
- Dehghani, Z., Noghreiyani, A.V., Nadafan, M. and Ara, M.M. (2017) 'Investigation of gamma-ray irradiation on molecular structure, optical properties and mass attenuation coefficients of colloidal gold nanoparticles', *Optical Materials*, 70, pp.99-105.
- Dell'Aglio, M., Mangini, V., Valenza, G., De Pascale, O., De Stradis, A., Natile, G., Arnesano, F. and De Giacomo, A. (2016) 'Silver and gold nanoparticles produced by pulsed laser ablation in liquid to investigate their interaction with ubiquitin', *Applied Surface Science*, 374, pp.297-304.
- Derkachova, A., Kolwas, K. and Demchenko, I. (2016) 'Dielectric function for gold in plasmonics applications: size dependence of plasmon resonance frequencies and damping rates for nanospheres', *Plasmonics*, 11(3), pp.941-951.
- Elsayed, K.A., Imam, H., Ahmed, M.A. and Ramadan, R. (2013) 'Effect of focusing conditions and laser parameters on the fabrication of gold nanoparticles via laser ablation in liquid', *Optics & Laser Technology*, 45, pp.495-502.
- Etchegoin, P. G., Le Ru, E. C. and Meyer, M. (2007) 'Erratum: "An analytic model for the optical properties of gold" [J. Chem. Phys. 125, 164705 (2006)]', *The Journal of Chemical Physics*, 127(18), p. 189901.
- Etchegoin, P.G., Le Ru, E.C. and Meyer, M. (2006) 'An analytic model for the optical properties of gold', *The Journal of Chemical Physics*, 125(16), p.164705.
- Eustis, S. and El-Sayed, M.A. (2006) 'Why gold nanoparticles are more precious than pretty gold: noble metal surface plasmon resonance and its enhancement of the radiative and nonradiative properties of nanocrystals of different shapes', *Chemical Society Reviews*, 35(3), pp.209-217.
- Falahati, M., Attar, F., Sharifi, M., Saboury, A.A., Salihi, A., Aziz, F.M., Kostova, I., Burda, C., Priece, P., Lopez-Sanchez, J.A. and Laurent, S. (2020) 'Gold nanomaterials as key suppliers in biological and chemical sensing, catalysis,

- and medicine', *Biochimica et Biophysica Acta (BBA)-General Subjects*, 1864(1), p.129435.
- Feis, A., Gellini, C., Salvi, P.R. and Becucci, M. (2014) 'Photoacoustic excitation profiles of gold nanoparticles', *Photoacoustics*, 2(1), pp.47-53.
- Frens, G. (1973) 'Controlled nucleation for the regulation of the particle size in monodisperse gold suspensions', *Nature Physical Science*, 241(105), pp.20-22.
- Gagui, S., Zaidi, B., Megdoud, Y., Hadjoudja, B., Chouial, B., Meradji, H., Ghemid, S. and Shekhar, C. (2020) 'Ab-initio study of the structural and optoelectronic properties of BaSe_{1-x}S_x alloys', *Computational Condensed Matter*, 22, p.e00433.
- Ghoshal, S.K., Awang, A., Sahar, M.R. and Arifin, R. (2015) 'Gold nanoparticles assisted surface enhanced Raman scattering and luminescence of Er³⁺ doped zinc–sodium tellurite glass', *Journal of Luminescence*, 159, pp.265-273.
- Ghoshal, S.K., Sahar, M.R., Dousti, M.R., Sharma, S., Rohani, M.S., Arifin, R. and Hamzah, K. (2012) 'Model for up-conversion luminescence in silver nanoparticles embedded erbium-doped tellurite glass', *Indian Journal of Pure & Applied Physics*, 50, pp. 555-565
- Ghoshal, S.K., Sahar, M.R., Rohani, M.S. and Sharma, S. (2011) 'Nanophotonics for 21st century', *In Optoelectronics-Devices and Applications. IntechOpen*.
- Giorgetti, E., Muniz-Miranda, M., Marsili, P., Scarpellini, D. and Giammanco, F. (2012) 'Stable gold nanoparticles obtained in pure acetone by laser ablation with different wavelengths', *Journal of Nanoparticle Research*, 14(1), p.648.
- Glantschnig, K. and Ambrosch-Draxl, C. (2010) 'Relativistic effects on the linear optical properties of Au, Pt, Pb and W', *New Journal of Physics*, 12(10), p.103048.
- Grady, N.K., Halas, N.J. and Nordlander, P. (2004) 'Influence of dielectric function properties on the optical response of plasmon resonant metallic nanoparticles', *Chemical Physics Letters*, 399(1-3), pp.167-171.
- Gupta, G., Nautiyal, T. and Auluck, S. (2004) 'Optical properties of the compounds BaTiO₃ and SrTiO₃', *Physical Review B*, 69(5), p.052101.
- Hao, F. and Nordlander, P. (2007) 'Efficient dielectric function for FDTD simulation of the optical properties of silver and gold nanoparticles', *Chemical Physics Letters*, 446(1-3), pp.115-118.

- Hohenberg, P. and Kohn, W. (1964) 'Inhomogeneous electron gas', *Physical Review*, 136. B864.
- Hong, S. and Li, X. (2013) 'Optimal size of gold nanoparticles for surface-enhanced Raman spectroscopy under different conditions', *Journal of Nanomaterials*, 2013.
- Horikoshi, S. and Serpone, N. (2013) 'Introduction to nanoparticles', *Microwaves in Nanoparticle Synthesis: Fundamentals and Applications*, pp.1-24.
- Huang, T. and Murray, R.W. (2001) 'Visible luminescence of water-soluble monolayer-protected gold clusters', *The Journal of Physical Chemistry B*, 105(50), pp.12498-12502.
- Huang, X. and El-Sayed, M.A. (2010) 'Gold nanoparticles: Optical properties and implementations in cancer diagnosis and photothermal therapy', *Journal of Advanced Research*, 1(1), pp.13-28.
- Isiyaku, A.K. and Ghoshal, S.K. (2016) 'Photoluminescence spectral features of silicon nanowires', *Jurnal Teknologi*, 78(3-2).
- Islam, M.N. and Kumar, S. (2003) 'Influence of surface states on the photoluminescence from silicon nanostructures', *Journal of Applied Physics*, 93(3), pp.1753-1759.
- Jain, P.K., Lee, K.S., El-Sayed, I.H. and El-Sayed, M.A. (2006) 'Calculated absorption and scattering properties of gold nanoparticles of different size, shape, and composition: applications in biological imaging and biomedicine', *The Journal of Physical Chemistry B*, 110(14), pp.7238-7248.
- Jiang, H. (2013) 'Band gaps from the Tran-Blaha modified Becke-Johnson approach: A systematic investigation', *The Journal of Chemical Physics*, 138(13), p.134115.
- Johnson, P.B. and Christy, R.W. (1972) 'Optical constants of the noble metals', *Physical Review B*, 6(12), p.4370.
- Jones, R.R., Hooper, D.C., Zhang, L., Wolverson, D. and Valev, V.K. (2019) 'Raman techniques: fundamentals and frontiers', *Nanoscale Research Letters*, 14(1), pp.1-34.
- Jones, T.E., Piccinin, S. and Stampfl, C. (2013) 'Relativity and the nobility of gold', *Materials Chemistry and Physics*, 141(1), pp.14-17.
- Kayang, K.W., Nyankson, E., Efavi, J.K., Apalangya, V.A., Adetunji, B.I., Gebreyesus, G., Tia, R., Abavare, E.K.K., Onwona-Agyeman, B. and Yaya,

- A. (2019) 'A comparative study of the interaction of nickel, titanium, palladium, and gold metals with single-walled carbon nanotubes: A DFT approach', *Results in Physics*, 12, pp.2100-2106.
- Khlebtsov, N.G. (2008) 'Determination of size and concentration of gold nanoparticles from extinction spectra', *Analytical Chemistry*, 80(17), pp.6620-6625.
- Kobayashi, Y., Correa-Duarte, M.A. and Liz-Marzán, L.M. (2001) 'Sol-gel processing of silica-coated gold nanoparticles', *Langmuir*, 17(20), pp.6375-6379.
- Kohn, W. and Sham, L.J. (1965) 'Self-consistent equations including exchange and correlation effects', *Physical Review*, 140(4A), p.A1133.
- Koller, D., Tran, F. and Blaha, P. (2011) 'Merits and limits of the modified Becke-Johnson exchange potential', *Physical Review B*, 83(19), p.195134.
- Koller, D., Tran, F. and Blaha, P. (2012) 'Improving the modified Becke-Johnson exchange potential', *Physical Review B*, 85(15), p.155109.
- Kreibig, U. and Vollmer, M. (2013) 'Optical properties of metal clusters', Vol. 25. *Springer Science & Business Media*.
- Kumar, C.S. ed. (2013) 'UV-VIS and photoluminescence spectroscopy for nanomaterials characterization', *Berlin, Heidelberg: Springer*.
- Kurelchuk, U.N., Borisyuk, P.V., Vasilyev, O.S. and Lebedinskii, Y.Y. (2017) 'DFT study of electronic properties of noble d-metallic surface structures', *Materials Today: Proceedings*, 4(12), pp.12343-12348.
- Laban, B., Ralević, U., Petrović, S., Leskovac, A., Vasić-Anićijević, D., Marković, M. and Vasić, V. (2020) 'Green synthesis and characterization of nontoxic L-methionine capped silver and gold nanoparticles', *Journal of Inorganic Biochemistry*, 204, p.110958.
- Lee, S.H., Jung, H.J., Lee, S.J., Theerthagiri, J., Kim, T.H. and Choi, M.Y. (2020) 'Selective synthesis of Au and graphitic carbon-encapsulated Au (Au@ GC) nanoparticles by pulsed laser ablation in solvents: Catalytic Au and acid-resistant Au@ GC nanoparticles', *Applied Surface Science*, 506, p.145006.
- Liao, H., Wen, W. and Wong, G.K. (2006) 'Photoluminescence from Au nanoparticles embedded in Au: oxide composite films', *Journal of the Optical Society of America B*, 23(12), pp.2518-2521.

- Lin, K.Q., Yi, J., Hu, S., Sun, J.J., Zheng, J.T., Wang, X. and Ren, B. (2016) ‘Intraband hot-electron photoluminescence from single silver nanorods’, *Acs Photonics*, 3(7), pp.1248-1255.
- Link, S. and El-Sayed, M.A. (1999) ‘Spectral properties and relaxation dynamics of surface plasmon electronic oscillations in gold and silver nanodots and nanorods’, *Journal of Physical Chemical B*, 103(1), pp. 8410–8426.
- Link, S. and El-Sayed, M.A. (2000) ‘Shape and size dependence of radiative, non-radiative and photothermal properties of gold nanocrystals’, *International Reviews in Physical Chemistry*, 19(3), pp.409-453.
- Liu, K., He, Z., Curtin, J.F., Byrne, H.J. and Tian, F. (2019) ‘A novel, rapid, seedless, in situ synthesis method of shape and size controllable gold nanoparticles using phosphates’, *Scientific Reports*, 9(1), pp.1-13.
- Liu, L. and Corma, A. (2018) ‘Metal catalysts for heterogeneous catalysis: from single atoms to nanoclusters and nanoparticles’, *Chemical Reviews*, 118(10), pp.4981-5079.
- Liu, X., Wang, Y., Eisenbach, M. and Stocks, G.M. (2018) ‘Fully-relativistic full-potential multiple scattering theory: A pathology-free scheme’, *Computer Physics Communications*, 224, pp.265-272.
- Long, P.D., Chien, D.T., Trung, N.T., Hieu, N.S., Van Cat, V. and Lam, V.D. (2017) ‘Plasmonic Effect Enhanced Photocurrent in Nanostructured TiO₂ Films Decorated with Gold Nanoparticles’, *Journal of Electronic Materials*, 46(7), pp.4448-4454.
- Lu, M., Zhu, H., Bazuin, C.G., Peng, W. and Masson, J.F. (2019) ‘Polymer-templated gold nanoparticles on optical fibers for enhanced-sensitivity localized surface plasmon resonance biosensors’, *ACS Sensors*, 4(3), pp.613-622.
- Luo, D., Wang, X., Zeng, S., Ramamurthy, G., Burda, C. and Basilion, J.P. (2019) Prostate-specific membrane antigen targeted gold nanoparticles for prostate cancer radiotherapy: does size matter for targeted particles?, *Chemical Science*, 10(35), pp.8119-8128.
- Maciulevičius, M., Vinčiūnas, A., Brikas, M., Butsen, A., Tarasenko, N., Tarasenko, N. and Račiukaitis, G. (2013) ‘Pulsed-laser generation of gold nanoparticles with on-line surface plasmon resonance detection’, *Applied Physics A*, 111(1), pp.289-295.

- Maiman, T.H. (1960) 'Stimulated optical radiation in ruby', *Nature*, 187(4736), pp.493-494.
- Matrane, I., Mazroui, M. and Boughaleb, Y. (2018) 'Diffusion and adsorption of Au and Pt adatoms on ideal and missing row reconstructed surfaces of Au (110): DFT and EAM calculations', *Surface Science*, 677, pp.83-89.
- Mätzler, C. (2002) 'MATLAB functions for Mie scattering and absorption', version 2. *IAP Res. Rep*, 8(1), p.9.
- Meija, J., Coplen, T.B., Berglund, M., Brand, W.A., De Bièvre, P., Gröning, M., Holden, N.E., Irrgeher, J., Loss, R.D., Walczyk, T. and Prohaska, T. (2016) 'Atomic weights of the elements 2013', *Pure and Applied Chemistry*, 88(3), pp.265-291.
- Mendivil Palma, M.I., Krishnan, B., Rodriguez, G.A.C., Das Roy, T.K., Avellaneda, D.A. and Shaji, S. (2016) 'Synthesis and properties of platinum nanoparticles by pulsed laser ablation in liquid', *Journal of Nanomaterials*, 2016.
- Menéndez-Manjón, A., Wagener, P. and Barcikowski, S. (2011) 'Transfer-matrix method for efficient ablation by pulsed laser ablation and nanoparticle generation in liquids', *The Journal of Physical Chemistry C*, 115(12), pp.5108-5114.
- Minoli, D. (2005) 'Nanotechnology applications to telecommunications and networking', *John Wiley & Sons*.
- Mohammed, Y.H., Sakrani, S.B. and Rohani, M.S. (2015) 'Improved structural features of Au-catalyzed silicon nanoneedles', *Superlattices and Microstructures*, 85, pp.849-858.
- Mooradian, A. (1969) 'Photoluminescence of metals', *Physical Review Letters*, 22(5), p.185.
- Moura, C.G., Pereira, R.S.F., Andritschky, M., Lopes, A.L.B., de Freitas Grilo, J.P., do Nascimento, R.M. and Silva, F.S. (2017) 'Effects of laser fluence and liquid media on preparation of small Ag nanoparticles by laser ablation in liquid', *Optics & Laser Technology*, 97, pp.20-28.
- Nainaa, F. and Ez-Zahraouy, H. (2018) 'First-principle study of structural, electronic and optical properties of Cu₂FeSnS₄ semiconductor', *Computational Condensed Matter*, 16, p.e00321.

- Nayef, U.M. and Khudhair, I.M. (2018) 'Synthesis of gold nanoparticles chemically doped with porous silicon for organic vapor sensor by using photoluminescence', *Optik*, 154, pp.398-404.
- Neddersen, J., Chumanov, G. and Cotton, T.M. (1993) 'Laser ablation of metals: a new method for preparing SERS active colloids', *Applied Spectroscopy*, 47(12), pp.1959-1964.
- Nedyalkov, N., Koleva, M.E., Nikov, R., Stankova, N.E., Iordanova, E., Yankov, G., Aleksandrov, L. and Iordanova, R. (2019) 'Tuning optical properties of noble metal nanoparticle-composed glasses by laser radiation', *Applied Surface Science*, 463, pp.968-975.
- Nikov, R.G., Nikolov, A.S., Nedyalkov, N.N., Atanasov, P.A., Alexandrov, M.T. and Karashanova, D.B. (2013) 'Processing condition influence on the characteristics of gold nanoparticles produced by pulsed laser ablation in liquids', *Applied Surface Science*, 274, pp.105-109.
- Nilsson, P.O., Norris, C. and Walldén, L. (1970) 'The electronic structure of gold studied by photoemission', *Physik der Kondensierten Materie*, 11(3), pp.220-230.
- Olson, J., Dominguez-Medina, S., Hoggard, A., Wang, L.Y., Chang, W.S. and Link, S. (2015) 'Optical characterization of single plasmonic nanoparticles', *Chemical Society Reviews*, 44(1), pp.40-57.
- Özdemir, E.G. and Merdan, Z. (2020) 'The effect of structural changes on the half metallic properties by using Tran Blaha modified Becke Johnson (TB_mBJ) method', *Journal of Magnetism and Magnetic Materials*, p.167198.
- Palazzo, G., Valenza, G., Dell'Aglio, M. and De Giacomo, A. (2017) 'On the stability of gold nanoparticles synthesized by laser ablation in liquids', *Journal of Colloid and Interface Science*, 489, pp.47-56.
- Palik, E.D. ed. (1998) 'Handbook of optical constants of solids', Vol. 1-4, *Academic press*.
- Parra, M.J.A. and Paradinas, S.S. (2014) 'Spectroscopic Techniques Based on the Use of Gold Nanoparticles', *In Comprehensive Analytical Chemistry*, 66, pp. 477-527.
- Patil, P.P., Phase, D.M., Kulkarni, S.A., Ghaisas, S.V., Kulkarni, S.K., Kanetkar, S.M., Ogale, S.B. and Bhide, V.G. (1987) 'Pulsed-laser-induced reactive

- quenching at liquid-solid interface: Aqueous oxidation of iron', *Physical Review Letters*, 58(3), p.238.
- Pattabi, M. and Pattabi, R.M. (2014) 'Photoluminescence from Gold and Silver Nanoparticles. In Nano Hybrids', *Trans Tech Publications Ltd*, 6, pp. 1-35.
- Pavia, D.L., Lampman, G.M., Kriz, G.S. and Vyvyan, J.A. (2008) 'Introduction to spectroscopy', *Cengage Learning*.
- Peck, J.A., Tait, C.D., Swanson, B.I. and Brown Jr, G.E. (1991) 'Speciation of aqueous gold (III) chlorides from ultraviolet/visible absorption and Raman/resonance Raman spectroscopies', *Geochimica et Cosmochimica Acta*, 55(3), pp.671-676.
- Peña-Rodríguez, O. (2017) 'Modelling the dielectric function of Au-Ag alloys', *Journal of Alloys and Compounds*, 694, pp.857-863.
- Perdew, J.P., Burke, K. and Ernzerhof, M. (1996) 'Generalized gradient approximation made simple', *Physical Review Letters*, 77(18), p.3865.
- Pyykko, P. (1988) 'Relativistic effects in structural chemistry', *Chemical Reviews*, 88(3), pp.563-594.
- Qi, W.H. and Wang, M.P. (2005) 'Size and shape dependent lattice parameters of metallic nanoparticles', *Journal of Nanoparticle Research*, 7(1), pp.51-57.
- Qian, X. and Park, H.S. (2010) 'The influence of mechanical strain on the optical properties of spherical gold nanoparticles', *Journal of the Mechanics and Physics of Solids*, 58(3), pp.330-345.
- Rafique, M., Rafique, M.S., Butt, S.H., Kalsoom, U., Afzal, A., Anjum, S. and Usman, A. (2017) 'Dependence of the structural optical and thermo-physical properties of gold nano-particles synthesized by laser ablation method on the nature of laser', *Optik*, 134, pp.140-148.
- Rameshe, B., Gnanapoongothai, T., Shanmugapriya, K., Murugan, R. and Palanivel, B. (2016) 'Theoretical Investigations on Electronic Structure, Structural Phase Stability and Optical Properties of Strontium Double Perovskites: Sr₂AMoO₆ (A= Mg, Zn)', *Materials Today: Proceedings*, 3(10), pp.4242-4248.
- Rangel, T., Kecik, D., Trevisanutto, P.E., Rignanese, G.M., Van Swygenhoven, H. and Olevano, V. (2012) 'Band structure of gold from many-body perturbation theory', *Physical Review B*, 86(12), p.125125.

- Riabinina, D., Zhang, J., Chaker, M., Margot, J. and Ma, D. (2012) 'Size control of gold nanoparticles synthesized by laser ablation in liquid media', *ISRN Nanotechnology*, 2012.
- Rioux, D., Vallières, S., Besner, S., Muñoz, P., Mazur, E. and Meunier, M. (2014) 'An analytic model for the dielectric function of Au, Ag, and their alloys', *Advanced Optical Materials*, 2(2), pp.176-182.
- Roduner, E. (2006) 'Size matters: why nanomaterials are different', *Chemical Society Reviews*, 35(7), pp.583-592.
- Rueden, C.T., Schindelin, J., Hiner, M.C., DeZonia, B.E., Walter, A.E., Arena, E.T. and Eliceiri, K.W. (2017) 'ImageJ2: ImageJ for the next generation of scientific image data', *BMC Bioinformatics*, 18(1), p.529.
- Sanna, S., Thierfelder, C., Wippermann, S., Sinha, T.P. and Schmidt, W.G. (2011) 'Barium titanate ground-and excited-state properties from first-principles calculations', *Physical Review B*, 83(5), p.054112.
- Scherpelz, P., Govoni, M., Hamada, I. and Galli, G. (2016) 'Implementation and validation of fully relativistic GW calculations: spin-orbit coupling in molecules, nanocrystals, and solids', *Journal of Chemical Theory and Computation*, 12(8), pp.3523-3544.
- Schwarz, K., Blaha, P. and Madsen, G.K. (2002) 'Electronic structure calculations of solids using the WIEN2k package for material sciences', *Computer Physics Communications*, 147(1-2), pp.71-76.
- Shabaninezhad, M. and Ramakrishna, G. (2019) 'Theoretical investigation of size, shape, and aspect ratio effect on the LSPR sensitivity of hollow-gold nanoshells', *The Journal of Chemical Physics*, 150(14), p.144116.
- Silva-De Hoyos, L.E., Sanchez-Mendieta, V., Camacho-Lopez, M.A., Trujillo-Reyes, J. and Vilchis-Nestor, A.R. (2020) 'Plasmonic and fluorescent sensors of metal ions in water based on biogenic gold nanoparticles', *Arabian Journal of Chemistry*, 13(1), pp.1975-1985.
- Smith, D.J. (2008) 'Ultimate resolution in the electron microscope?', *Materials Today*, 11, pp.30-38.
- Smith, N.V. (1974) 'Photoemission spectra and band structures of d-band metals. III. Model band calculations on Rh, Pd, Ag, Ir, Pt, and Au', *Physical Review B*, 9(4), p.1365.

- Smith, P.V., Hermanowicz, M., Shah, G.A. and Radny, M.W. (2012) ‘Spin–orbit and modified Becke–Johnson potential effects on the electronic properties of bulk Ge: A density functional theory study’, *Computational Materials Science*, 54, pp.37-42.
- Soares, J.A. (2014) ‘Introduction to optical characterization of materials’, *In Practical Materials Characterization*, pp. 43-92.
- Sönnichsen, C. (2001) ‘Plasmons in metal nanostructures’, *Doctoral Dissertation, lmu*.
- Städele, M., Moukara, M., Majewski, J.A., Vogl, P. and Görling, A. (1999) ‘Exact exchange Kohn-Sham formalism applied to semiconductors’, *Physical Review B*, 59(15), p.10031.
- Suárez, J.A., Plata, J.J., Márquez, A.M. and Sanz, J.F. (2016) ‘Structural, electronic and optical properties of copper, silver and gold sulfide: a DFT study’, *Theoretical Chemistry Accounts*, 135(3), p.70.
- Taghizadeh, S., Alimardani, V., Roudbali, P.L., Ghasemi, Y. and Kaviani, E. (2019) ‘Gold nanoparticles application in liver cancer’, *Photodiagnosis and Photodynamic Therapy*, 25, pp.389-400.
- Theileis, V. and Bross, H. (2000) ‘Relativistic modified augmented plane wave method and its application to the electronic structure of gold and platinum’, *Physical Review B*, 62(20), p.13338.
- Tran, F. and Blaha, P. (2009) ‘Accurate band gaps of semiconductors and insulators with a semilocal exchange-correlation potential’, *Physical Review Letters*, 102(22), p.226401.
- Tran, F., Blaha, P. and Schwarz, K. (2007) ‘Band gap calculations with Becke–Johnson exchange potential’, *Journal of Physics: Condensed Matter*, 19(19), p.196208.
- Urban, A. (2010) ‘Optothermal manipulation of phospholipid membranes with gold nanoparticles’, *Doctoral Dissertation, lmu*.
- Vedhanayagam, M., Nair, B.U. and Sreeram, K.J. (2019) ‘Effect of functionalized gold nanoparticle on collagen stabilization for tissue engineering application’, *International Journal of Biological Macromolecules*, 123, pp.1211-1220.
- Vinod, M. and Gopchandran, K.G. (2014) ‘Au, Ag and Au: Ag colloidal nanoparticles synthesized by pulsed laser ablation as SERS substrates’, *Progress in Natural Science: Materials International*, 24(6), pp.569-578.

- Vinod, M., Jayasree, R.S. and Gopchandran, K.G. (2017) 'Synthesis of pure and biocompatible gold nanoparticles using laser ablation method for SERS and photothermal applications', *Current Applied Physics*, 17(11), pp.1430-1438.
- Wang, R., Chen, K. and Ge, G. (2014) 'A simple spectroscopic method for the quantification of gold nanoparticle number concentration in water and fetal bovine serum solutions', *Chinese Science Bulletin*, 59(16), pp.1816-1821.
- Werner, W.S., Glantschnig, K. and Ambrosch-Draxl, C. (2009) 'Optical constants and inelastic electron-scattering data for 17 elemental metals', *Journal of Physical and Chemical Reference Data*, 38(4), pp.1013-1092.
- Werner, W.S., Went, M.R., Vos, M., Glantschnig, K. and Ambrosch-Draxl, C. (2008) 'Measurement and density functional calculations of optical constants of Ag and Au from infrared to vacuum ultraviolet wavelengths', *Physical Review B*, 77(16), p.161404.
- Yan, Z. and Chrisey, D.B. (2012) 'Pulsed laser ablation in liquid for micro-/nanostructure generation', *Journal of Photochemistry and Photobiology C: Photochemistry Reviews*, 13(3), pp.204-223.
- Yu, J., Nan, J. and Zeng, H. (2017) 'Size control of nanoparticles by multiple-pulse laser ablation', *Applied Surface Science*, 402, pp.330-335.
- Zamiri, R., Zakaria, A., Ahangar, H.A., Darroudi, M., Zamiri, G., Rizwan, Z. and Drummen, G.P. (2013) 'The effect of laser repetition rate on the LASiS synthesis of biocompatible silver nanoparticles in aqueous starch solution', *International Journal of Nanomedicine*, 8, p.233.
- Zeng, H., Du, X.W., Singh, S.C., Kulinich, S.A., Yang, S., He, J. and Cai, W. (2012) 'Nanomaterials via laser ablation/irradiation in liquid: a review', *Advanced Functional Materials*, 22(7), pp.1333-1353.
- Zhang, D., Gökce, B. and Barcikowski, S. (2017a) 'Laser synthesis and processing of colloids: fundamentals and applications', *Chemical Reviews*, 117(5), pp.3990-4103.
- Zhang, J., Claverie, J., Chaker, M. and Ma, D. (2017b) 'Colloidal metal nanoparticles prepared by laser ablation and their applications', *ChemPhysChem*, 18(9), pp.986-1006.
- Zheng, J., Zhou, C., Yu, M. and Liu, J. (2012) 'Different sized luminescent gold nanoparticles', *Nanoscale*, 4(14), pp.4073-4083.

Zhou, M., Higaki, T., Hu, G., Sfeir, M.Y., Chen, Y., Jiang, D.E. and Jin, R. (2019)
‘Three-orders-of-magnitude variation of carrier lifetimes with crystal phase
of gold nanoclusters’, *Science*, 364(6437), pp.279-282.

LIST OF PUBLICATIONS

- Alluhaybi, H. A., Ghoshal, S. K., Alsobhi, B. O. and Shamsuri, W. N. W. (2019) 'Electronic and optical correlation effects in bulk gold: Role of spin-orbit coupling', *Computational Condensed Matter*. Elsevier B.V., 18, p. e00360.
- Alluhaybi, H. A., Ghoshal, S. K., Shamsuri, W. N. W., Alsobhi, B. O., Salim, A. A. and Krishnan, G. (2019) 'Pulsed laser ablation in liquid assisted growth of gold nanoparticles: Evaluation of structural and optical features', *Nano-Structures and Nano-Objects*. Elsevier B.V., 19, p. 100355.
- Alluhaybi, H. A., Ghoshal, S. K., Alsobhi, B. O. and Wan Shamsuri, W. N. (2019) 'Visible photoluminescence from gold nanoparticles: A basic insight', *Optik*. Elsevier, 192(March), p. 162936.